There are relatively few reports about the regulation of SXR expression to date. Aouabdi *et al.* (2006) reported the presence of a PPAR alpha binding site 2.2 kb upstream of the transcription start site in human SXR. This site corresponded to the induction site with clofibrate in the rat and they further confirmed its importance using human liver cancer cell line (Huh7). Jung *et al.* (2006) reported the presence of four FXR binding sites in intron 2 of the mouse SXR gene that were required for FXR regulation of SXR expression. This intron 2 region is completely intact in our hSXRki mouse. Therefore, the regulation by FXR should be preserved in our mice.

Compared to the previously generated humanized Alb-SXR, SXR BAC, and hSXR genome mice, we contend that our hSXRki mouse has an advantage because the human-mouse chimeric gene is expressed in the same tissues and at similar levels to endogenous SXR in WT mice under control of the mouse promoter. This feature would make this model suitable not only for systemic toxicity but also toxicity at various stages of development of the embryo and fetus, maturation of infant, and of senescence, where the *cis* and *trans* regulations might be critical in its regulation (Sarsero *et al.*, 2004) (Konopka *et al.*, 2009). Thus, we believe that our system has a broader application range for toxicological studies.

ACKNOWLEDGMENTS

The authors thank Ms. Yuko Matsushima, Mr. Masaki Tsuji, Ms. Maki Otsuka, Mr. Yusuke Furukawa, Mr. Kouichi Morita, Ms. Maki Abe, and Ms. Shinobu Watanabe for technical support. This study was supported in part by the Health Sciences Research Grants H19-Toxico-Shitei-001 from the Ministry of Health, Labour and Welfare, Japan.

REFERENCES

Aouabdi, S., Gibson, G. and Plant, N. (2006): Transcriptional regulation of the PXR gene: identification and characterization of a functional peroxisome proliferator-activated receptor alpha binding site within the proximal promoter of PXR. Drug Metab. Dispos., **34**, 138-144.

Bertilsson, G., Heidrich, J., Svensson, K., Asman, M., Jendeberg, L., Sydow-Bäckman, M., Ohlsson, R., Postlind, H., Blomquist, P. and Berkenstam, A. (1998): Identification of a human nuclear receptor defines a new signaling pathway for CYP3A induction. Proc. Natl. Acad. Sci., USA, **95**, 12208-12213.

Blumberg, B., Sabbagh, W.Jr., Juguilon, H., Bolado, J.Jr., van Meter, C.M., Ong, E.S. and Evans, R.M. (1998): SXR, a novel steroid and xenobiotic-sensing nuclear receptor. Genes. Dev., **12**, 3195-3205.

Jung, D., Mangelsdorf, D.J. and Meyer, U.A. (2006): Pregnane X receptor is a target of farnesoid X receptor. J. Biol. Chem., **281**, 19081-19091.

Kanno, J., Aisaki, K., Igarashi, K., Nakatsu, N., Ono, A., Kodama, Y. and Nagao, T. (2006): "Per cell" normalization method for mRNA measurement by quantitative PCR and microarrays. BMC genomics, **7**, 64.

Konopka, G., Bomar, J.M., Winden, K., Coppola, G., Jonsson, Z.O., Gao, F., Peng, S., Preuss, T.M., Wohlschlegel, J.A. and Geschwind, D.H. (2009): Human-specific transcriptional regulation of CNS development genes by FOXP2. Nature, **462**, 213-217.

Lehmann, J.M., McKee, D.D., Watson, M.A., Willson, T.M., Moore, J.T. and Kliewer, S.A. (1998): The human orphan nuclear receptor PXR is activated by compounds that regulate CYP3A4 gene expression and cause drug interactions. J. Clin. Invest., **102**, 1016-1023.

Ma, X., Shah, Y., Cheung, C., Guo, G.L., Feigenbaum, L., Krausz, K.W., Idle, J.R. and Gonzalez, F.J. (2007): The PREgnane X receptor gene-humanized mouse: a model for investigating drug-drug interactions mediated by cytochromes P450 3A. Drug Metab. Dispos., **35**, 194-200.

Saga, Y., Hata, N., Koseki, H. and Taketo, M.M. (1997): Mesp2: a novel mouse gene expressed in the presegmented mesoderm and essential for segmentation initiation. Genes. Dev., **11**, 1827-1839.

Saga, Y., Miyagawa-Tomita, S., Takagi, A., Kitajima, S., Miyazaki, J. and Inoue, T. (1999): MesP1 is expressed in the heart precursor cells and required for the formation of a single heart tube. Development, **126**, 3437-3447.

Sakai, K. and Miyazaki, J. (1997): A transgenic mouse line that retains Cre recombinase activity in mature oocytes irrespective of the cre transgene transmission. Biochem. Biophys. Res. Commun., **237**, 318-324.

Sarsero, J.P., Li, L., Holloway, T.P., Voullaire, L., Gazeas, S., Fowler, K.J., Kirby, D.M., Thorburn, D.R., Galle, A., Cheema, S., Koenig, M., Williamson, R. and Ioannou, P.A. (2004): Human BAC-mediated rescue of the Friedreich ataxia knockout mutation in transgenic mice. Mamm. Genome., **15**, 370-382.

Scheer, N., Ross, J., Rode, A., Zevnik, B., Niehaves, S., Faust, N. and Wolf, C.R. (2008): A novel panel of mouse models to evaluate the role of human pregnane X receptor and constitutive androstane receptor in drug response. J. Clin. Invest., **118**, 3228-3239.

Suzuki, T., Akimoto, M., Mandai, M., Takahashi, M. and Yoshimura, N. (2005): A new PCR-based approach for the preparation of RNA probe. J. Biochem. Biophys. Methods., **62**, 251-258.

Tirona, R.G., Leake, B.F., Podust, L.M. and Kim, R.B. (2004): Identification of amino acids in rat pregnane X receptor that determine species-specific activation. Mol. Pharmacol., **65**, 36-44.

Watkins, R.E., Wisely, G.B., Moore, L.B., Collins, J.L., Lambert, M.H., Williams, S.P., Willson, T.M., Kliewer, S.A. and Redinbo, M.R. (2001): The human nuclear xenobiotic receptor PXR: structural determinants of directed promiscuity. Science, **292**, 2329-2333.

Xie, W., Barwick, J.L., Downes, M., Blumberg, B., Simon, C.M., Nelson, M.C., Neuschwander-Tetri, B.A., Brunt, E.M., Guzelian, P.S. and Evans, R.M. (2000): Humanized xenobiotic response in mice expressing nuclear receptor SXR. Nature, **406**, 435-439.

Yagi, T., Tokunaga, T., Furuta, Y., Nada, S., Yoshida, M., Tsukada, T., Saga, Y., Takeda, N., Ikawa, Y. and Aizawa, S. (1993): A novel ES cell line, TT2, with high germline-differentiating potency. Anal. Biochem., **214**, 70-76.

Zhou, C., Tabb, M.M., Sadatrafiei, A., Grün, F. and Blumberg, B. (2004) Tocotrienols activate the steroid and xenobiotic receptor, SXR, and selectively regulate expression of its target genes. Drug Metab. Dispos., **32**, 1075-1082.

Evaluation of Breast Cancer Resistance Protein Function in Hepatobiliary and Renal Excretion Using PET with ^{11}C-SC-62807

Tadayuki Takashima[1], Chunyong Wu[2], Misato Takashima-Hirano[1], Yumiko Katayama[1], Yasuhiro Wada[1], Masaaki Suzuki[1], Hiroyuki Kusuhara[2], Yuichi Sugiyama[3], and Yasuyoshi Watanabe[1]

[1]RIKEN Center for Molecular Imaging Science, Kobe, Japan; [2]Laboratory of Molecular Pharmacokinetics, Graduate School of Pharmaceutical Sciences, The University of Tokyo, Tokyo, Japan; and [3]Sugiyama Laboratory, RIKEN Innovation Center, RIKEN Research Cluster for Innovation, Yokohama Bio Industry Center, Yokohama, Japan

A quantitative PET imaging method was used to assess the in vivo kinetics of hepatobiliary and renal excretion of the breast cancer resistance protein (Bcrp) substrate ^{11}C-SC-62807 in mice. **Methods:** Serial abdominal PET scans were collected in wild-type and Bcrp knockout (*Bcrp*$^{-/-}$) mice after intravenous injection of ^{11}C-SC-62807. Venous blood samples and PET images were obtained at frequent intervals up to 30 min after radiotracer administration. Dynamic PET data were analyzed to determine the canalicular and brush-border efflux clearances in the liver and kidney ($CL_{int,bile,liver}$ and $CL_{int,urine,kidney}$, respectively). **Results:** SC-62807 is an in vitro substrate of mouse Bcrp and human BCRP. Radioactivity associated with ^{11}C-SC-62807 was predominantly found in the blood, liver, bile, and urine 30 min after administration. Both biliary and urinary excretion of radioactivity was markedly lower in *Bcrp*$^{-/-}$ mice than in wild-type mice, suggesting greater systemic exposure in *Bcrp*$^{-/-}$ mice. Both the $CL_{int,bile,liver}$ and the $CL_{int,urine,kidney}$ were significantly lower in *Bcrp*$^{-/-}$ mice (74% ± 10% and 99% ± 1% lower than controls, respectively). We also found that ^{11}C-SC-62807 is a substrate of the organic anion-transporting polypeptides OATP1B1 and OATP1B3 in vitro. **Conclusion:** The present study demonstrated that Bcrp plays a significant role in the efflux of ^{11}C-SC-62807 in mouse liver and kidney. We also demonstrated the feasibility of PET using ^{11}C-SC-62807 to study the activity of BCRP in humans.

Key Words: breast cancer resistance protein; organic anion-transporting polypeptide; positron emission tomography; hepatobiliary transport; renal excretion

J Nucl Med 2013; 54:267–276
DOI: 10.2967/jnumed.112.110254

Drug transporters play an important role in drug disposition and may influence therapeutic efficacy or development of adverse drug reactions (*1–3*). The breast cancer resistance protein (Bcrp, rodents; BCRP/*ABCG2*, humans) is a member of the adenosine triphosphate (ATP)–binding cassette transporter G family and mediates the efflux transport of endobiotics and xenobiotics coupled with ATP hydrolysis (*4–6*). BCRP is expressed in various normal tissues, including liver, kidney, brain, placenta, and intestine, where it is expressed on the brush-border membranes of epithelial cells (*7*). Cumulative in vivo studies, particularly involving Bcrp knockout (*Bcrp*$^{-/-}$) mice, have demonstrated the important role BCRP plays in drug disposition, limiting oral absorption and penetration into the brain and testis (*8*), and mediating biliary and urinary excretion of xenobiotics such as pitavastatin and methotrexate (*1,9–11*). Pharmacogenomic studies focusing on a single nucleotide polymorphism frequently observed in Asians (421C>A) elucidated the importance of BCRP in systemic exposure to orally administered sulfasalazine and rosuvastatin (*12,13*). Because of the lack of a suitable probe, the role of BCRP in the elimination of BCRP substrates from the systemic circulation and their distribution in the brain has not been investigated. Furthermore, because BCRP eliminates uric acid, mutations and single nucleotide polymorphisms in this protein make it a risk factor for gout and are thus drawing increasing research interest (*14*). The many important roles played by BCRP make it a subject of major clinical interest.

PET is a powerful noninvasive molecular imaging technique that provides high sensitivity and good spatiotemporal resolution, enabling determination of the tissue concentration of drugs labeled with a positron-emitting radionuclide (*15–17*). The usefulness of transporter probes for molecular imaging has been demonstrated through in vivo phenotypic measurements of altered hepatobiliary transport of organic anion-transporting polypeptide (Oatp, rodents; OATP, humans) and multidrug resistance-associated protein 2 (Mrp2, rodents; MRP2, humans) in preclinical and

Received Jun. 20, 2012; revision accepted Aug. 23, 2012.
For correspondence or reprints contact: Tadayuki Takashima, Molecular Probe Dynamics Laboratory, RIKEN Center for Molecular Imaging Science, 6-7-3 Minatojima-minamimachi, Chuo-ku, Kobe, Hyogo 650-0047, Japan.
E-mail: ttakashima@riken.jp
Published online Jan. 3, 2013

clinical tests using ^{99m}Tc-mebrofenin (*18*) and 15*R*-^{11}C-TIC-Me (*19,20*). Recently, functional PET probes for Bcrp and P-glycoprotein, such as ^{11}C-elacridar and ^{11}C-gefitinib, have been described for use in the noninvasive in vivo evaluation of these proteins at the blood–brain barrier (BBB) (*21,22*). However, because the major elimination pathway of these probes is metabolism, they cannot be used to evaluate efflux activity in the liver and kidney.

SC-62807 is the major metabolite of celecoxib (a selective cyclooxygenase-2 inhibitor) and is produced by CYP2C9 (*23*). Because SC-62807 contains a carboxylate group and does not undergo further metabolism, we hypothesized that SC-62807 would be a good probe for certain efflux transporters in the liver, and we synthesized ^{11}C-SC-62807 for this purpose (Fig. 1). We previously demonstrated that in rats ^{11}C-SC-62807 is rapidly excreted into the bile without further metabolism (*24*). In this study, we elucidated the predominant role of Bcrp in the efflux of SC-62807 into the bile and urine in mice and demonstrate the feasibility of using PET to evaluate BCRP activity in humans.

MATERIALS AND METHODS

Celecoxib carboxylic acid (SC-62807) was purchased from Toronto Research Chemicals Inc. ^{11}C-SC-62807 was synthesized according to previously reported procedures (*24*). The chemical purity of ^{11}C-SC-62807 was determined by measuring the ultraviolet absorbance at 254 nm. The radiochemical purity was greater than 98%, and the specific radioactivity was 14 ± 10 GBq/μmol at the time of injection. All chemicals and solvents used for labeling synthesis were analytic grade.

Animals

Male wild-type FVB and *Bcrp*$^{-/-}$ mice were purchased from Taconic Inc. (age, 6–12 wk, weight, 22–30 g). Mice were maintained in a temperature- and light-controlled environment with ad libitum access to standard food and tap water. All experimental protocols were approved by the Ethics Committee on Animal Care and Use of the Center for Molecular Imaging Science at RIKEN and were performed in accordance with the *Guide for the Care and Use of Laboratory Animals (25).*

Determination of ATP-Dependent Uptake of SC-62807 by Transporter-Expressing Membrane Vesicles

Membrane vesicles were prepared as described previously from HEK293 cells infected with adenoviruses expressing mouse Bcrp (mBcrp), human BCRP (hBCRP), and green fluorescent protein (GFP) (control) (*26*) and with recombinant adenoviruses containing human MRP2 and tetracycline-responsive transcriptional activator (*27*). A rapid filtration technique was used to assess ATP-dependent uptake (*26*). Samples were quantified using liquid chromatography–tandem mass spectrometry. The level of ATP-dependent uptake was calculated by subtracting the uptake into vesicles in the presence of adenosine monophosphate (AMP) from that in the presence of ATP. Kinetic parameters were calculated using the Michaelis–Menten equation:

$$v = \frac{V_{max} \times S}{K_m + S}, \quad \text{Eq. 1}$$

where v represents the uptake velocity of the substrate, S represents the substrate concentration in the medium, K_m represents the Michaelis constant, and V_{max} represents the maximum uptake velocity. The nonlinear least-squares method was used for fitting (Damping Gauss–Newton method algorithm) with the MULTI program (*28*).

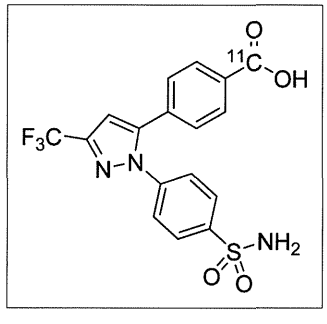

FIGURE 1. Chemical structure of ^{11}C-SC-62807.

PET Studies

All PET scans were obtained using a microPET Focus220 scanner (Siemens) designed for laboratory animals. Mice were anesthetized and maintained with a mixture of 1.5% isoflurane and oxygen and then placed on the PET scanner gantry. An emission scan was performed after intravenous bolus injection of ^{11}C-SC-62807 (158 ± 32 MBq/kg) via a catheter inserted into the tail. The bolus injections contained 0.23 ± 0.19 μg of SC-62807 per animal. An emission scan was obtained in 3-dimensional list mode for 30 min and sorted into 26 dynamic sinograms according to the following sequence: 12 × 5, 3 × 20, 3 × 60, 5 × 120, and 3 × 300 s. Blood was sampled via the tail vein at the following time points: 2, 5, 15, 30, and 60 min after radiotracer administration. In addition, the biodistribution in a separate group of mice was also determined. After blood and urine sampling, blood flow was terminated by exsanguination via aortic puncture, and the liver and kidneys were quickly removed, weighed, and assayed for regional radioactivity using a 1470 Wizard automatic γ-counter (PerkinElmer). The radioactivity measured in each sample was decay-corrected to the injection time and expressed as percentage dose per tissue or percentage dose per milliliter of blood, normalized to the injected radioactivity.

Radiometabolite Analysis

Radiometabolites in the blood, urine, liver, and bile of a separate group of mice (n = 2) were analyzed using radiometric high-performance liquid chromatography. Blood and urine were collected 15 min after the mice received an intravenous injection of ^{11}C-SC-62807 (~211 ± 21 MBq/kg), and bile was sampled from the gallbladder 30 min after injection. To sample liver tissue, blood flow was terminated 15 min after administration, and the liver was quickly removed and homogenized. Sample preparation and chromatographic separation were performed as described previously (*24*).

Analysis of PET Data

PET images were reconstructed using microPET Manager 2.4.1.1 (Siemens) by standard 2-dimensional filtered backprojection using a ramp filter with a cutoff at the Nyquist frequency. Regions of interest representing the liver and the intestines were delineated using PMOD software (version 3.0; PMOD Technologies Ltd.), as described previously (*19*). In this PET analysis, the sum of the radioactivity in the gallbladder and intestine corresponds

to the radioactivity in the bile secreted to these tissues because a conventional biodistribution study revealed that the bile radioactivity sampled from rats with bile duct cannulas is comparable to that in the intestine as determined by PET image analysis (*24*). A time profile of the radioactivity in each tissue was constructed by normalizing decay-corrected time-radioactivity measurements to the injected dose (percentage dose) of ^{11}C-SC-62807.

The biliary secretion clearance ($CL_{bile,blood,0-30\ min}$) and renal clearance ($CL_{renal,blood,0-30\ min}$) with respect to the blood radioactivity concentration were calculated using the following equations:

$$CL_{bile,blood,0-30min} = X_{bile,0-30min}/AUC_{blood,0-30min} \quad \text{Eq. 2}$$

and

$$CL_{urine,blood,0-30min} = X_{urine,0-30min}/AUC_{blood,0-30min}, \quad \text{Eq. 3}$$

where X represents the amount of radioactivity secreted into the bile or urine between 0 and 30 min, and $AUC_{blood,0-30\ min}$ represents the area under the blood radioactivity concentration–time curve for the time period 0–30 min.

The apparent tissue–to–blood area under the curve (AUC) ratio ($K_{p,liver,AUC}$ or $K_{p,kidney,AUC}$) was calculated using the following equation:

$$K_{p,tissue,AUC} = AUC_{tissue,0-30min}/AUC_{blood,0-30min}, \quad \text{Eq. 4}$$

where $AUC_{tissue,0-30\ min}$ represents the area under the tissue radioactivity concentration–time curve for the time period 0–30 min.

Canalicular efflux clearance ($CL_{int,bile,liver}$) was estimated by integration plot analysis using noninvasive measurements of radioactivity in the liver and bile encompassing about the first 27.5 min after ^{11}C-SC-62807 administration, during which the plot shows linear regression. Kidney brush-border efflux clearance with respect to the kidney concentration ($CL_{int,urine,kidney}$) was estimated by integration plot analysis using the radioactivity in the kidney and urine encompassing about the first 6 min after ^{11}C-SC-62807 administration for wild-type mice and the first 27.5 min after administration for *Bcrp*$^{-/-}$ mice. Biliary efflux and kidney brush-border efflux clearances were calculated using the following equations:

$$X_{t,bile} = CL_{int,bile,liver} \times AUC_{0-t,liver} + X_{E,bile} \quad \text{Eq. 5}$$

and

$$X_{t,urine} = CL_{int,urine,kidney} \times AUC_{0-t,kidney} + X_{E,urine}, \quad \text{Eq. 6}$$

where $X_{t,bile}$ and $X_{t,urine}$ represent the amount of radioactivity excreted into the bile and urine, respectively, at time t as determined by PET image analysis. The areas under the hepatic and renal concentration–time curves from time 0 to time t are represented by $AUC_{0-t,liver}$ and $AUC_{0-t,kidney}$, respectively. The $CL_{int,bile,liver}$ and $CL_{int,urine,kidney}$ can be obtained from the slopes of plots of $X_{t,bile}$ versus $AUC_{0-t,liver}$ and $X_{t,urine}$ versus $AUC_{0-t,kidney}$, respectively. Values for $X_{E,urine}$ and $X_{E,bile}$ were determined from the y-intercept of the respective integration plots, representing the initial distribution in these regions of interest (tissues) at time 0.

Uptake by Transporter-Expressing HEK293 Cells

OATP1B1- and OATP1B3-expressing HEK293 cells were established previously (*29*). The transport study was performed as described previously (*29*). Briefly, cells were seeded onto 12-well plates coated with poly-L-lysine and poly-L-ornithine. After 2 d, the culture medium was replaced with medium supplemented with 5 mM sodium butyrate, and cells were incubated for 24 h before the transport study to induce transporter expression. Cells were then washed and preincubated with Krebs–Henseleit buffer. Uptake was initiated by adding buffer containing radiolabeled compounds or unlabeled SC-62807 and terminated at the designated time by adding ice-cold buffer after removal of the incubation buffer. To assess uptake of radiolabeled compounds, cells were solubilized with 0.2N NaOH and kept overnight at 4°C. After neutralization with HCl, aliquots were transferred to scintillation vials and radioactivity associated with the cells and incubation buffer was measured using a liquid scintillation counter (LS6000SE; Beckman Coulter) after the addition of scintillation cocktail (Clear-sol I; Nacalai Tesque). To assess uptake of SC-62807, cells were solubilized in H_2O by sonication on ice. Aliquots of the cell lysate were extracted with ethyl acetate, and sulfasalazine was used as the internal standard. After centrifugation, the supernatants were evaporated, reconstituted with 10 mM ammonium acetate/methanol (40:60, v/v), and quantitatively analyzed using liquid chromatography–tandem mass spectrometry. The remaining cell lysate was used to determine the protein concentration using the Lowry method with bovine serum albumin as a standard.

Estimating Contribution of OATP1B1 and OATP1B3 to SC-62807 Uptake by Human Hepatocytes

The contribution of OATP1B1 and OATP1B3 to SC-62807 uptake by human hepatocytes was estimated using relative activity factor analysis, as described in detail elsewhere (*28,29*). Briefly, relative activity factors for OATP1B1 and OATP1B3 (R_{1B1} or R_{1B3}) were calculated as the uptake clearance in human hepatocytes ($CL_{hepatocyte,ref}$) divided by $CL_{1B1,ref}$ or $CL_{1B3,ref}$ using the reference compounds ^{3}H-E_1S and ^{3}H-CCK-8 for OATP1B1 and OATP1B3, respectively:

$$R_{1B1} = \frac{CL_{hepatocyte,ref}}{CL_{1B1,ref}}, \quad \text{Eq. 7}$$

$$R_{1B3} = \frac{CL_{hepatocyte,ref}}{CL_{1B3,ref}}. \quad \text{Eq. 8}$$

The uptake clearance of SC-62087 in hepatocytes ($CL_{hepatocytes,SC}$) was estimated as the product of the R values (R_{1B1} and R_{1B3}) and uptake clearance of SC-62087 in OATP1B1- and OATP1B3-expressing HEK293 cells ($CL_{OATP1B1,SC}$ and $CL_{OATP1B3,SC}$) using the following equation:

$$CL_{hepatocyte,SC} = R_{1B1} \times CL_{1B1,SC} + R_{1B3} \times CL_{1B3,SC}. \quad \text{Eq. 9}$$

The contributions of OATP1B1 and OATP1B3 are defined as the product of R_{1B1} and $CL_{1B1,SC}$ divided by $CL_{hepatocyte,SC}$ and the product of R_{1B3} and $CL_{1B3,SC}$ divided by $CL_{hepatocyte,SC}$, respectively.

Statistical Analysis

Data are presented as the mean ± SD for 3–4 determinations. The statistical significance of differences between groups was de-

termined using the Student 2-tailed unpaired t test. Statistical significance was set at a P value of less than 0.05.

RESULTS

ATP-Dependent Uptake of SC-62807 into mBcrp- or hBCRP-Expressing Membrane Vesicles

Uptake of SC-62807 by membrane vesicles expressing mBcrp or hBCRP was markedly stimulated in the presence of ATP but not in the presence of AMP or in vesicles prepared from control cells (Fig. 2A). Uptake of SC-62807 was saturable and followed Michaelis–Menten kinetics, with K_m and V_{max} values of 19.9 ± 3.9 μM and 435 ± 50 pmol/min/mg of protein, respectively, for mBcrp and 10.4 ± 1.73 μM and 2,263 ± 204 pmol/min/mg of protein, respectively, for hBCRP (Fig. 2B).

Distribution of Radioactivity in Abdominal Region and Blood of Mice After Administration of ^{11}C-SC-62807

Radioactivity localized primarily in the liver and kidneys within 2 min of ^{11}C-SC-62807 administration in both wild-type and *Bcrp*$^{-/-}$ mice and subsequently moved to the intestine (derived from bile) or the urinary bladder (derived from urine) in wild-type mice by 30 min after administration (Fig. 3A). In contrast, translocation of radioactivity to the intestine and urinary bladder was markedly delayed in *Bcrp*$^{-/-}$ mice (Fig. 3B).

Mouse abdominal region tissue and blood radioactivity time profiles are shown in Figure 4. A maximum of 35% ± 8% and 14% ± 3% of the dose was distributed in the liver and kidney, respectively, of wild-type mice by 2 min after administration, after which the amount of radioactivity declined rapidly. In contrast, radioactivity in the liver and kidney of *Bcrp*$^{-/-}$ mice reached a maximum at 4 and 18 min, respectively, and then decreased gradually. Radioactivity in the bile (sum of gallbladder and intestine) and urine of wild-type mice increased until 30 min, reaching 48% ± 3% and 26% ± 5% of the dose, respectively, whereas the level of radioactivity in the bile and the urine was much lower. A separate conventional biodistribution study revealed that in wild-type and *Bcrp*$^{-/-}$ mice, the radiotracer is distributed primarily in the liver (34% and 44% of dose, respectively) and to a lesser degree in the kidneys (3% and 16% of dose) and urine (7% and 0.02% of dose) at 5 min after administration. At 30 min, radioactivity in the liver, kidney, and urine of wild-type and *Bcrp*$^{-/-}$ mice was 10% and 25%, 0.4% and 14%, and 5% and 9% of the dose, respectively. These data were comparable to the PET data. Radioactivity in the blood decreased rapidly in wild-type mice but decreased only slightly and then remained constant in *Bcrp*$^{-/-}$ mice. The $AUC_{blood,0-30\ min}$ for *Bcrp*$^{-/-}$ mice (93% ± 19% of the dose × min/mL) was 2.2-fold higher than that for wild-type mice (42% ± 18% of the dose × min/mL) (Table 1). The liver-to-blood AUC ratio ($K_{p,liver,AUC}$) was lower in *Bcrp*$^{-/-}$ mice than in wild-type mice; however, the difference was not statistically significant. The kidney-to-blood AUC ratio ($K_{p,kidney,AUC}$) was significantly higher in *Bcrp*$^{-/-}$ mice than in wild-type mice ($P < 0.01$) (Fig. 4; Table 1). High-performance liquid chromatography analysis revealed that almost 100% of the radioactivity in the blood, liver, bile, and urine represented unchanged ^{11}C-SC-62807 (Fig. 5), indicating that in mice ^{11}C-SC-62807 is rapidly eliminated without further metabolism via hepatobiliary and renal excretion.

Canalicular Efflux and Kidney Brush-Border Efflux Clearance of ^{11}C-SC−62807 in Mice

Clearance of radioactivity via canalicular and kidney brush-border efflux ($CL_{int,bile,liver}$ and $CL_{int,urine,kidney}$,

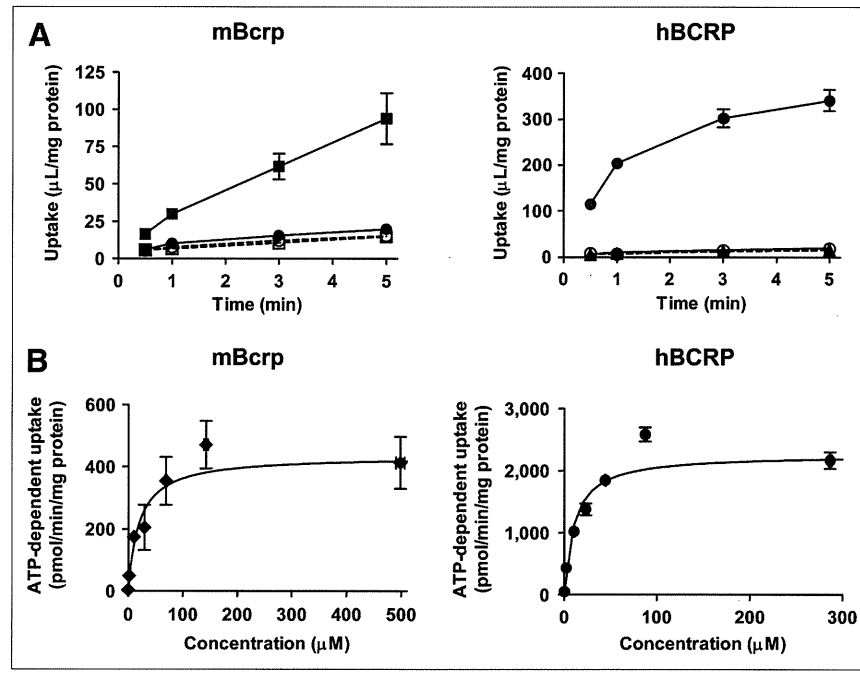

FIGURE 2. Time profiles of SC-62807 uptake by mBcrp, hBCRP, and control vesicles. Uptake of SC-62807 (2 μM) into membrane vesicles was determined in presence of ATP (closed symbols) or AMP (open symbols). Uptake was terminated at designated time. (A) Squares and circles connected using solid and broken lines represent uptake by transporter (mBcrp or hBCRP) and membrane vesicles (control) expressing green fluorescent protein, respectively. (B) Uptake of various concentrations (0.22, 2.18, 10.8, 29.7, 68.9, 142, and 498 μM for mBcrp and 0.23, 2.21, 10.6, 23.3, 44.5, 87.8, and 287 μM for hBCRP) of SC-62807 into transporter-expressing membrane vesicles for 1 min. Velocity of ATP-dependent uptake by mBcrp- and hBCRP-expressing vesicles was fitted to Michaelis–Menten equation using nonlinear regression analysis, and solid line in (B) represents fitted curve. Each point represents mean ± SE (n = 3).

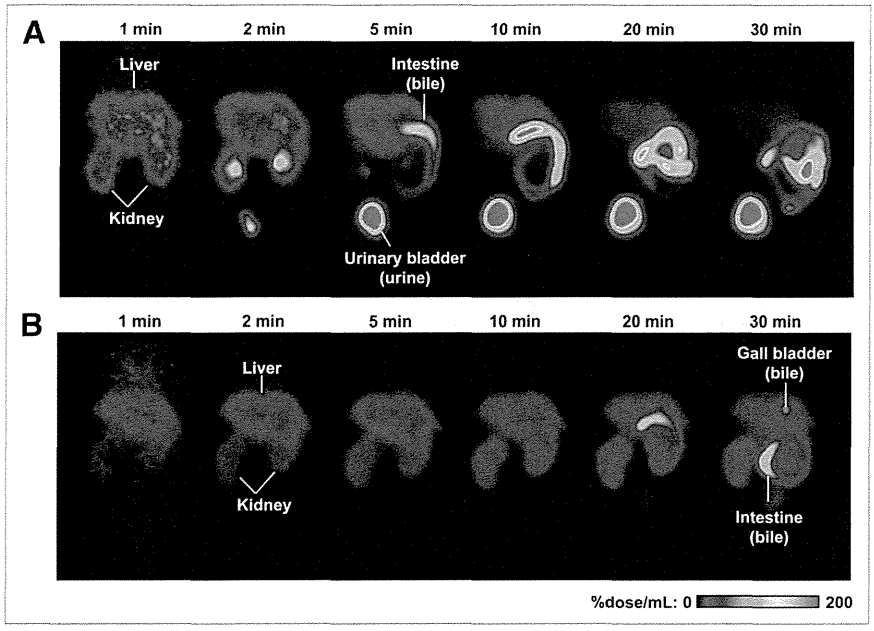

FIGURE 3. Color-coded PET images of abdominal region of wild-type and *Bcrp*$^{-/-}$ mice after administration of ^{11}C-SC−62807. Coronal maximum-intensity-projection PET images of radioactivity in abdominal region of wild-type (A) and *Bcrp*$^{-/-}$ (B) mice were captured at 1, 2, 5, 10, 20, and 30 min after intravenous bolus administration of ^{11}C-SC-62807.

respectively) was determined by integration plot analysis (Fig. 6). The integration plots used to determine $CL_{int,bile,liver}$ for wild-type and *Bcrp*$^{-/-}$ mice were linear 10 min after ^{11}C-SC-62807 administration (Fig. 6A). The $CL_{int,bile,liver}$ for *Bcrp*$^{-/-}$ mice was significantly lower (by 74% ± 10%; $P < 0.01$) (1.2 ± 0.1 mL/min/kg) than that for wild-type mice (4.5 ± 0.8 mL/min/kg) (Table 1). The integration plots used to determine $CL_{int,urine,kidney}$ were linear within 6 min of ^{11}C-SC-62807 administration for wild-type mice and within 30 min for *Bcrp*$^{-/-}$ mice (Fig. 6B). The $CL_{int,urine,kidney}$ for *Bcrp*$^{-/-}$ mice (0.12 ± 0.07 mL/min/kg) was significantly lower (by 99% ± 1%; $P < 0.001$) than for wild-type mice (13 ± 2 mL/min/kg) (Table 1). The difference in $CL_{int,bile,liver}$ between wild-type and *Bcrp*$^{-/-}$ mice was smaller than the difference

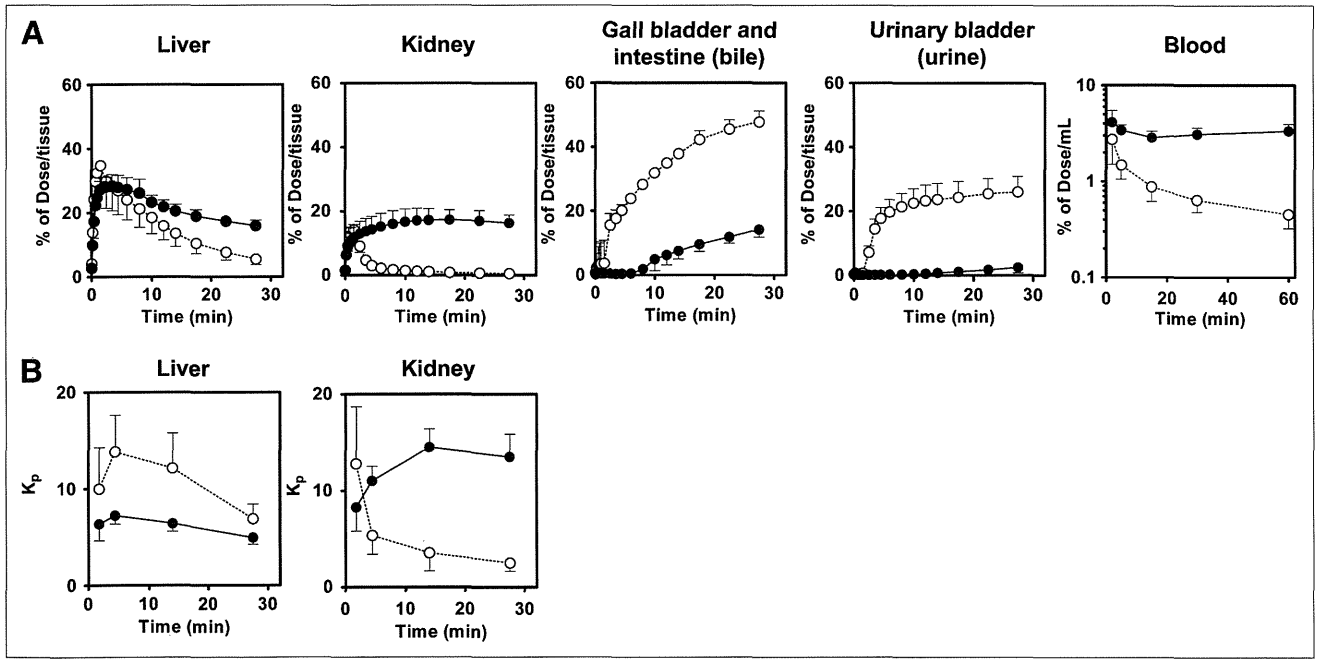

FIGURE 4. Radioactivity time profiles in tissue and blood after administration of ^{11}C-SC-62807 to wild-type and *Bcrp*$^{-/-}$ mice. (A) Radioactivity time profiles in liver, kidney, bile, urine, and blood of wild-type and *Bcrp*$^{-/-}$ mice determined using PET and blood sampling within 60 min of administration of ^{11}C-SC-62807. (B) Time profiles of liver-to-blood and kidney-to-blood radioactivity ratios (K_p) in wild-type and *Bcrp*$^{-/-}$ mice. Each symbol with bar represents mean ± SD ($n = 4$). Open and closed symbols represent wild-type and *Bcrp*$^{-/-}$ mice, respectively.

TABLE 1
Pharmacokinetic Parameters of ^{11}C-SC-62807 in Wild-Type and *Bcrp*$^{-/-}$ Mice

Pharmacokinetic parameter	Wild-type mice	*Bcrp*$^{-/-}$ mice	Ratio of *Bcrp*$^{-/-}$ to wild-type
$AUC_{blood,0-30\ min}$ (% dose × min/mL)	42 ± 18	93 ± 19*	2.2 ± 1.1
$AUC_{liver,0-30\ min}$ (% dose × min/mL)	369 ± 85	535 ± 76†	1.5 ± 0.4
$AUC_{kidney,0-30\ min}$ (% dose × min/mL)	170 ± 36	1,119 ± 126‡	6.6 ± 1.6
$K_{p,liver,AUC}$ (mL/g of liver)	8.8 ± 3.0	5.6 ± 0.8	0.64 ± 0.24
$K_{p,kidney,AUC}$ (mL/g of kidney)	4.0 ± 1.3	11.7 ± 2.3*	2.9 ± 1.1
$X_{bile,0-30\ min}$ (% dose)	48 ± 3	13 ± 2‡	0.28 ± 0.04
$X_{urine,0-30\ min}$ (% dose)	26 ± 5	3.0 ± 1.7‡	0.11 ± 0.07
$CL_{bile,blood,0-30\ min}$ (mL/min/kg)	48 ± 19	5.1 ± 1.6†	0.11 ± 0.05
$CL_{renal,blood,0-30\ min}$ (mL/min/kg)	25 ± 8	1.2 ± 0.7*	0.046 ± 0.033
$CL_{int,bile,liver}$ (mL/min/kg)	4.5 ± 0.8	1.2 ± 0.1*	0.26 ± 0.05
$CL_{int,urine,kidney}$ (mL/min/kg)	13 ± 2	0.12 ± 0.07*	0.0088 ± 0.0051

*Unpaired *t* test, $P < 0.01$.
†Unpaired *t* test, $P < 0.05$.
‡Unpaired *t* test, $P < 0.001$.
Each value represents mean ± SD (n = 3–4). Statistically significant difference was observed for several pharmacokinetic parameters in *Bcrp*$^{-/-}$ mice, compared with wild-type.

in $CL_{bile,blood,0-30\ min}$, whereas the difference in $CL_{int,urine,kidney}$ between wild-type and *Bcrp*$^{-/-}$ mice was much larger than the difference in $CL_{renal,blood,0-30\ min}$.

Estimation of SC-62807 Uptake Clearance and Contribution of OATP1B1 and OATP1B3 in Human Hepatocytes

Uptake of SC-62807 by OATP1B1- and OATP1B3-expressing cells and vector-transfected HEK293 cells (control) is shown in Figure 7. Uptake of SC-62807 was significantly higher in OATP-expressing cells than in control cells and was saturable, with K_m and V_{max} values of 260 ± 138 μM and 319 ± 133 pmol/min/mg of protein, respectively, for OATP1B1 and 19.8 ± 2.56 μM and 205 ± 16.2 pmol/min/mg of protein, respectively, for OATP1B3. The uptake clearance of SC-62807 mediated by OATP1B1 and OATP1B3 in human hepatocytes was estimated by comparing the uptake clearance of reference compounds (^{3}H-E_1S and ^{3}H-CCK-8) in transfectants and hepatocytes (Table 2). Clearance of SC-62807 mediated by OATP1B1

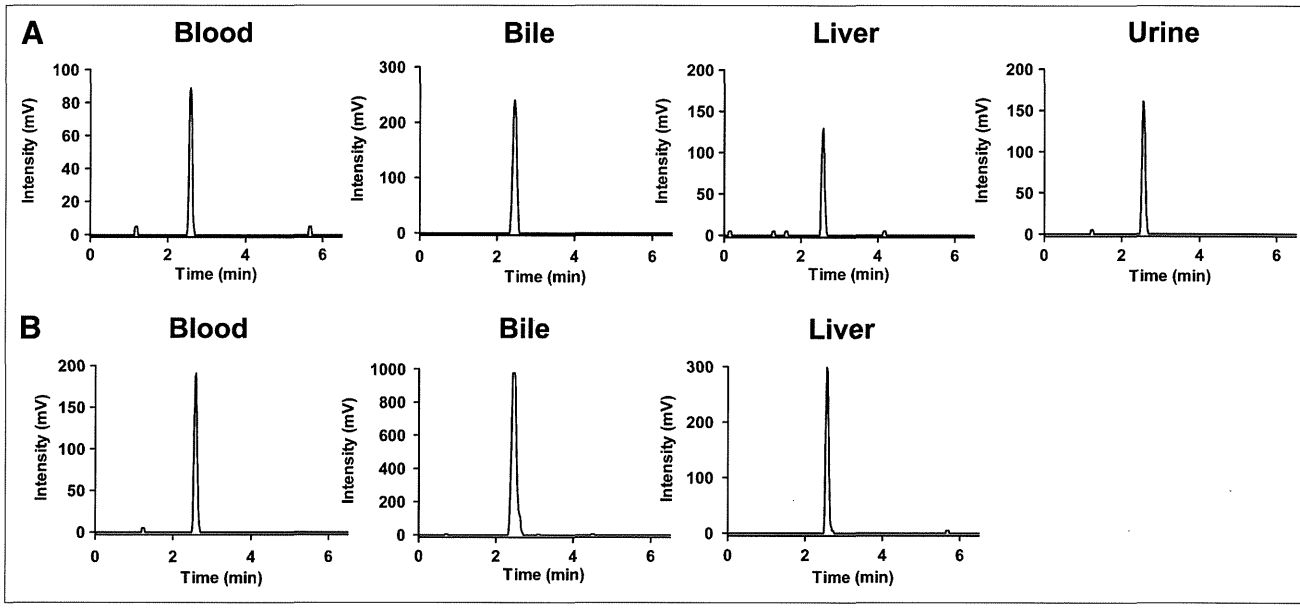

FIGURE 5. Representative high-performance liquid chromatograms of blood, bile, liver, and urine extracts from wild-type and *Bcrp*$^{-/-}$ mice after administration of ^{11}C-SC-62807. (A) Radiochromatograms of blood extracts sampled at 15 min, bile extracts sampled from gallbladder at 30 min, liver extracts sampled at 15 min, and urine extracts sampled 15 min after administration of ^{11}C-SC-62807 to wild-type mice. (B) Radiochromatograms of blood extracts sampled at 15 min, bile extracts sampled from gallbladder at 30 min, and liver extracts sampled 15 min after administration of ^{11}C-SC-62807 to *Bcrp*$^{-/-}$ mice. Radioactivity in urine of *Bcrp*$^{-/-}$ mice was below detection limit for radiometric high-performance liquid chromatography.

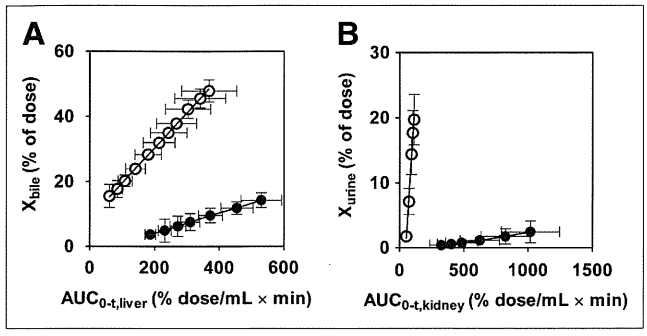

FIGURE 6. Integration plots for determination of canalicular efflux and renal secretion of total radioactivity in wild-type and *Bcrp*$^{-/-}$ mice. Integration plots were drawn for calculation of canalicular (A) and kidney brush-border (B) efflux of ^{11}C-SC-62807 in wild-type and *Bcrp*$^{-/-}$ mice. Each symbol with bar represents mean ± SD (n = 4). Open and closed symbols represent wild-type and *Bcrp*$^{-/-}$ mice, respectively.

and OATP1B3 was similar in human hepatocytes as determined by R values (Table 2).

DISCUSSION

BCRP is an ATP-binding cassette transporter involved in biliary and renal excretion. The purpose of this study was to clarify the utility of ^{11}C-SC-62807 as a PET probe for analyzing the function of Bcrp in biliary and renal excretion in experimental animals and to demonstrate the feasibility of using ^{11}C-SC-62807 to assess BCRP function in humans. PET studies with ^{11}C-SC-62807 were designed to examine the kinetics of hepatobiliary transport and renal excretion in mice.

In vitro transport studies using mBcrp- and hBCRP-expressing membrane vesicles showed that SC-62807 is a substrate for BCRP in both mice and humans. This finding prompted us to investigate the tissue distribution and significance of Bcrp in the elimination of SC-62807 from the systemic circulation because Bcrp is normally expressed in the canalicular membrane of hepatocytes and the brush-border membrane on the proximal tubules in rodents (*1*) as well as in the BBB and blood–placenta barrier.

PET revealed that ^{11}C-SC-62807 is excreted into the bile and urine. Because radiometabolite analyses indicated that radioactivity associated with ^{11}C-SC-62807 metabolites is negligible in the blood, liver, bile, and urine of mice, the total radioactivity represents the unchanged form. After intravenous bolus injection, ^{11}C-SC-62807 is predominantly excreted into the bile and, to a slightly lesser extent, into the urine. About 74% of the radioactivity was recovered in the bile and urine of wild-type mice within 30 min of administration. The ^{11}C-SC-62807 $CL_{renal,blood,0\text{–}30\ min}$ was greater than the reported creatinine clearance value (8.7 ± 2.0 mL/min/kg) (*30*), indicating that tubular secretion contributes significantly to renal excretion.

Because BCRP is expressed in the apical membrane, its transport activity is tightly associated with the intrinsic efflux activity across the canalicular and brush-border membranes ($CL_{int,bile,liver}$ and $CL_{int,urine,kidney}$). An advantage of PET is that it enables noninvasive monitoring of the tissue concentration to determine these parameters. Our PET analysis demonstrated that both biliary and renal excretion of ^{11}C-SC-62807 is significantly reduced in *Bcrp*$^{-/-}$ mice, leading to prolonged systemic exposure to ^{11}C-SC-62807. The marked decrease in both $CL_{int,bile,liver}$ and $CL_{int,urine,kidney}$ in

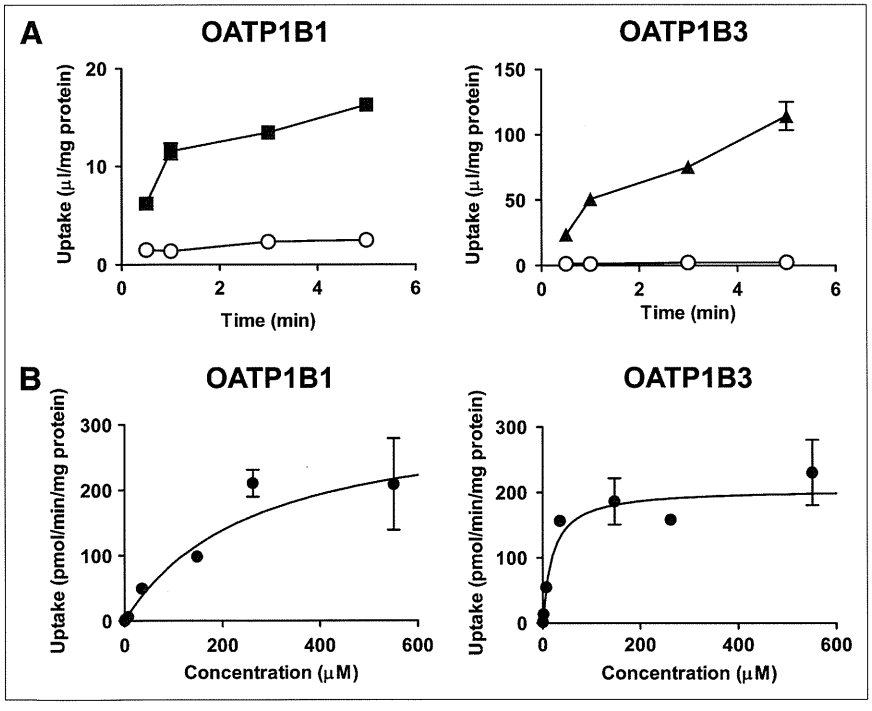

FIGURE 7. Time profiles of SC-62807 uptake by OATP1B1- and OATP1B3-expressing HEK293 cells and dependence of uptake on concentration. (A) Uptake of SC-62807 by human OATP1B1- (■) and OATP1B3 (▲)-expressing HEK293 and mock cells (○) was determined at 37°C at designated time. (B) Uptake of SC-62807 into OATP1B1- and OATP1B3-expressing HEK293 cells was determined with varying concentrations of SC-62807 at 37°C for 1.5 min. OATP1B1- and OATP1B3-mediated transport was calculated by subtracting uptake in vector-transfected control cells from that in transporter-expressing cells. Data were fitted to Michaelis–Menten equation using nonlinear least-squares method, and each solid line represents fitted curve. Each point represents mean ± SE (n = 3).

TABLE 2
Contribution of OATP1B1 and OATP1B3 to Hepatic Uptake of SC-62807 in Humans

	Reference compounds			SC-62807		
Lot no. and transporter	(1) Human hepatocytes* ($CL_{hepatocyte,ref}$ [μL/min/10^6 cells])	(2) OATP1B1-HEK or OATP1B3-HEK ($CL_{1B1,ref}$ or $CL_{1B3,ref}$ [μL/min/mg protein])	(3) R_{1B1} and R_{1B3}: (1)/(2) ($CL_{hepatocyte,ref}/CL_{1B1,ref}$ or $CL_{hepatocyte,ref}/CL_{1B3,ref}$)	(4) OATP1B1-HEK or OATP1B3-HEK ($CL_{1B1,SC}$ or $CL_{1B3,SC}$ [μL/min/mg protein])	Human hepatocytes (3) × (4) ($CL_{hepatocyte,SC}$ [μL/min/10^6 cells])	Contribution (%)
OCF						
OATP1B1	110	311 ± 25.8	0.353	10.2	3.60	30.2
OATP1B3	7.89	47.0 ± 5.48	0.168	49.4	8.30	69.8
094						
OATP1B1	134	311 ± 25.8	0.430	10.2	4.38	54.3
OATP1B3	3.50	47.0 ± 5.48	0.0745	49.4	3.68	45.7
ETR						
OATP1B1	57.7	311 ± 25.8	0.185	10.2	1.89	47.0
OATP1B3	2.02	47.0 ± 5.48	0.0430	49.4	2.12	53.0

*These data are cited from previous report (*28*) in which uptake of reference compounds (^{3}H-E_1S for OATP1B1 and ^{3}H-CCK-8 for OATP1B3) were determined in 3 lots of cryopreserved hepatocytes (lot name: OCF, 094, and ETR).

Relative activity factors for OATP1B1 and OATP1B3 (R_{1B1} and R_{1B3}, respectively) were defined using uptake of reference compounds in OATP1B1- and OATP1B3-expressing HEK293 cells (OATP1B1- and OATP1B3-HEK, respectively) determined in this study ($CL_{1B1,ref}$ or $CL_{1B3,ref}$). OATP1B1- and OATP1B3-mediated uptake of SC-62087 in hepatocytes were estimated as product of R_{1B1} and $CL_{1B1,SC}$ and R_{1B1} and $CL_{1B1,SC}$, respectively. Contribution was calculated as ratio of OATP-mediated uptake and $CL_{hepatocyte,SC}$. Details of calculation are described in "Materials and Methods" section.

Bcrp$^{-/-}$ mice clearly indicates that the predominant contribution of Bcrp to efflux of ^{11}C-SC-62807 into the bile and urine. The transporter Mrp2 is indispensable to the efflux of most anionic drugs into the bile. SC-62807 was also shown to be an in vitro substrate for Mrp2 using an uptake study involving MRP2-expressing membrane vesicles. However, the V_{max}/K_m (5.6 ± 1.5 μL/min/mg of protein) was much lower than that for BCRP-expressing vesicles (218 ± 41 μL/min/mg of protein). There was only a slight decrease in the radioactivity excreted into the bile in Mrp2-deficient rats, compared with normal rats (data not shown). These results confirmed the specificity of SC-62807 for Bcrp in canalicular efflux.

Consistent with the marked reduction in efflux into the urine, the ^{11}C-SC-62807 $K_{p,kidney}$ was significantly higher in *Bcrp*$^{-/-}$ mice than in wild-type mice. Despite the marked reduction in $CL_{int,bile,liver}$, however, the $K_{p,liver,AUC}$ was lower in *Bcrp*$^{-/-}$ mice, possibly due either to a low contribution of canalicular efflux to the net efflux from hepatocytes or to adaptive regulation caused by a Bcrp defect. The transporter Mrp3 is expressed on the sinusoidal membrane of hepatocytes, where it mediates the sinusoidal efflux of anionic drugs and glucuronide conjugates into the blood. Sinusoidal efflux mediated by Mrp3 may contribute significantly to net hepatocytic efflux, thereby attenuating the impact of Bcrp defects on the liver-to-plasma ratio. A reduction in influx mediated by an unknown mechanism or elevation in sinusoidal efflux may also explain the discrepancy, although there are no reports concerning adaptive regulation in the expression of drug transporters in the liver of *Bcrp*$^{-/-}$ mice. We found that SC-62807 is a good in vitro substrate of OATP1B1 and OATP1B3 (Table 2). It is quite possible that rodent isoforms can mediate hepatic uptake of SC-62807. Further investigation is necessary to elucidate the mechanism underlying the discrepancy.

We also conducted ^{11}C-SC-62807 PET of mouse brain regions to demonstrate the utility of the technique for examining Bcrp function at the BBB. Brain penetration of ^{11}C-SC-62807 was low in both wild-type and *Bcrp*$^{-/-}$ mice, with the apparent tissue–to–blood concentration ratio (K_p) values around 0.03 (Supplemental Fig. 1; supplemental materials are available online only at http://jnm.snmjournals.org). Generally, anionic drugs have low distribution volumes in the brain, presumably because of high protein binding in the plasma and low membrane permeability of the BBB. Thus, we concluded that the use of this probe for examining Bcrp function at the BBB may be impractical because of the likelihood of poor transport across the BBB.

PET enables the direct noninvasive measurement of intrinsic efflux across the canalicular and brush-border membranes. Using PET, we detected a marked reduction in canalicular and brush-border efflux of the radioactivity associated with ^{11}C-SC-62807 in *Bcrp*$^{-/-}$ mice, demonstrating the feasibility of clinical investigations of BCRP variation using ^{11}C-SC-62807 as a radiotracer. It was reported that SC-62807, which is produced by oxidation of the antiinflammatory drug celecoxib, is found predominantly in the feces and urine after oral celecoxib administration in humans and that the amount of the glucuronide conjugate metabolite is low in both feces and urine (*31*), suggesting that ^{11}C-SC-62807 should be minimally metabolized in humans when administered as an intravenous injection. The fact that SC-62807 is a good substrate of OATP1B1 and OATP1B3 in vitro suggests that SC-62807 is efficiently taken up by the liver from the blood circulation. In humans, SC-62807 is most likely excreted into the bile by transporters. These characteristics fulfill the conditions required for in vivo PET. Clinical studies with ^{11}C-SC-62807 could elucidate the importance of BCRP in the disposition of drugs in humans and help resolve questions over interindividual differences in BCRP activity in the liver caused by genetic polymorphisms and sex differences.

CONCLUSION

We demonstrated the utility of noninvasive PET using ^{11}C-SC-62807 as a radiotracer for the functional characterization of Bcrp, a protein responsible for biliary and renal excretion. We also showed the feasibility of using this technique to assess BCRP-associated membrane transport in hepatobiliary and renal excretion in humans.

DISCLOSURE

The costs of publication of this article were defrayed in part by the payment of page charges. Therefore, and solely to indicate this fact, this article is hereby marked "advertisement" in accordance with 18 USC section 1734. This work was supported by a Grant-in-Aid for Young Scientists (B) (KAKENHI 21790171) from the Ministry of Education, Culture, Sports, Science and Technology (MEXT), Japanese government. This work was also supported by a Grant-in-Aid for Scientific Research on Innovative Areas HD-Physiology (23136101) from the Ministry of Education, Science, and Culture of Japan. No potential conflict of interest relevant to this article was reported.

ACKNOWLEDGMENTS

We are indebted to Emi Hayashinaka, Tomotaka Shingaki, and Kiyoshi Kyono of the RIKEN Center for Molecular Imaging Science; Masahiro Kurahashi of Sumitomo Heavy Industry Accelerator Service Ltd.; and Miyuu Yokochi and Sumito Ito of the Graduate School of Pharmaceutical Sciences, The University of Tokyo, for their expert technical support.

REFERENCES

1. Jonker JW, Buitelaar M, Wagenaar E, et al. The breast cancer resistance protein protects against a major chlorophyll-derived dietary phototoxin and protoporphyria. *Proc Natl Acad Sci USA.* 2002;99:15649–15654.
2. Schinkel AH, Mol CA, Wagenaar E, van Deemter L, Smit JJ, Borst P. Multidrug resistance and the role of P-glycoprotein knockout mice. *Eur J Cancer.* 1995;31A:1295–1298.
3. Cascorbi I. Role of pharmacogenetics of ATP-binding cassette transporters in the pharmacokinetics of drugs. *Pharmacol Ther.* 2006;112:457–473.

4. Doyle LA, Ross DD. Multidrug resistance mediated by the breast cancer resistance protein BCRP (ABCG2). *Oncogene.* 2003;22:7340–7358.
5. Allen JD, Schinkel AH. Multidrug resistance and pharmacological protection mediated by the breast cancer resistance protein (BCRP/ABCG2). *Mol Cancer Ther.* 2002;1:427–434.
6. Chu XY, Kato Y, Niinuma K, Sudo KI, Hakusui H, Sugiyama Y. Multispecific organic anion transporter is responsible for the biliary excretion of the camptothecin derivative irinotecan and its metabolites in rats. *J Pharmacol Exp Ther.* 1997;281:304–314.
7. van Herwaarden AE, Schinkel AH. The function of breast cancer resistance protein in epithelial barriers, stem cells and milk secretion of drugs and xenotoxins. *Trends Pharmacol Sci.* 2006;27:10–16.
8. Enokizono J, Kusuhara H, Ose A, Schinkel AH, Sugiyama Y. Quantitative investigation of the role of breast cancer resistance protein (Bcrp/Abcg2) in limiting brain and testis penetration of xenobiotic compounds. *Drug Metab Dispos.* 2008;36:995–1002.
9. Hirano M, Maeda K, Matsushima S, Nozaki Y, Kusuhara H, Sugiyama Y. Involvement of BCRP (ABCG2) in the biliary excretion of pitavastatin. *Mol Pharmacol.* 2005;68:800–807.
10. Mao Q, Unadkat JD. Role of the breast cancer resistance protein (ABCG2) in drug transport. *AAPS J.* 2005;7:E118–E133.
11. Breedveld P, Zelcer N, Pluim D, et al. Mechanism of the pharmacokinetic interaction between methotrexate and benzimidazoles: potential role for breast cancer resistance protein in clinical drug-drug interactions. *Cancer Res.* 2004;64:5804–5811.
12. Yamasaki Y, Ieiri I, Kusuhara H, et al. Pharmacogenetic characterization of sulfasalazine disposition based on NAT2 and ABCG2 (BCRP) gene polymorphisms in humans. *Clin Pharmacol Ther.* 2008;84:95–103.
13. Zhang W, Yu BN, He YJ, et al. Role of BCRP 421C>A polymorphism on rosuvastatin pharmacokinetics in healthy Chinese males. *Clin Chim Acta.* 2006;373:99–103.
14. Matsuo H, Takada T, Ichida K, et al. Identification of ABCG2 dysfunction as a major factor contributing to gout. *Nucleosides Nucleotides Nucleic Acids.* 2011;30:1098–1104.
15. Pysz MA, Gambhir SS, Willmann JK. Molecular imaging: current status and emerging strategies. *Clin Radiol.* 2010;65:500–516.
16. Bergström M, Grahnen A, Langstrom B. Positron emission tomography microdosing: a new concept with application in tracer and early clinical drug development. *Eur J Clin Pharmacol.* 2003;59:357–366.
17. Willmann JK, van Bruggen N, Dinkelborg LM, Gambhir SS. Molecular imaging in drug development. *Nat Rev Drug Discov.* 2008;7:591–607.
18. Ghibellini G, Leslie EM, Pollack GM, Brouwer KL. Use of tc-99m mebrofenin as a clinical probe to assess altered hepatobiliary transport: integration of in vitro, pharmacokinetic modeling, and simulation studies. *Pharm Res.* 2008;25:1851–1860.
19. Takashima T, Nagata H, Nakae T, et al. Positron emission tomography studies using (15*R*)-16-m-[^{11}C]tolyl-17,18,19,20-tetranorisocarbacyclin methyl ester for the evaluation of hepatobiliary transport. *J Pharmacol Exp Ther.* 2010;335:314–323.
20. Takashima T, Kitamura S, Wada Y, et al. PET imaging-based evaluation of hepatobiliary transport in humans with (15*R*)-^{11}C-TIC-Me. *J Nucl Med.* 2012;53:741–748.
21. Kawamura K, Yamasaki T, Konno F, et al. Evaluation of limiting brain penetration related to P-glycoprotein and breast cancer resistance protein using [^{11}C]GF120918 by PET in mice. *Mol Imaging Biol.* 2011;13:152–160.
22. Kawamura K, Yamasaki T, Yui J, et al. In vivo evaluation of P-glycoprotein and breast cancer resistance protein modulation in the brain using [^{11}C]gefitinib. *Nucl Med Biol.* 2009;36:239–246.
23. Tang C, Shou M, Mei Q, Rushmore TH, Rodrigues AD. Major role of human liver microsomal cytochrome P450 2C9 (CYP2C9) in the oxidative metabolism of celecoxib, a novel cyclooxygenase-II inhibitor. *J Pharmacol Exp Ther.* 2000;293:453–459.
24. Takashima-Hirano M, Takashima T, Katayama Y, et al. Efficient sequential synthesis of PET Probes of the COX-2 inhibitor [^{11}C]celecoxib and its major metabolite [^{11}C]SC-62807 and in vivo PET evaluation. *Bioorg Med Chem.* 2011;19:2997–3004.
25. *Guide for the Care and Use of Laboratory Animals.* Bethesda, MD: National Institutes of Health; 1985. NIH publication 86-23.
26. Kondo C, Suzuki H, Itoda M, et al. Functional analysis of SNPs variants of BCRP/ABCG2. *Pharm Res.* 2004;21:1895–1903.
27. Hirouchi M, Suzuki H, Itoda M, et al. Characterization of the cellular localization, expression level, and function of SNP variants of MRP2/ABCC2. *Pharm Res.* 2004;21:742–748.
28. Yamaoka K, Tanigawara Y, Nakagawa T, Uno T. A pharmacokinetic analysis program (multi) for microcomputer. *J Pharmacobiodyn.* 1981;4:879–885.
29. Hirano M, Maeda K, Shitara Y, Sugiyama Y. Contribution of OATP2 (OATP1B1) and OATP8 (OATP1B3) to the hepatic uptake of pitavastatin in humans. *J Pharmacol Exp Ther.* 2004;311:139–146.
30. Mizuno N, Suzuki M, Kusuhara H, et al. Impaired renal excretion of 6-hydroxy-5,7-dimethyl-2-methylamino-4-(3-pyridylmethyl) benzothiazole (E3040) sulfate in breast cancer resistance protein (BCRP1/ABCG2) knockout mice. *Drug Metab Dispos.* 2004;32:898–901.
31. Paulson SK, Hribar JD, Liu NW, et al. Metabolism and excretion of [^{14}C]celecoxib in healthy male volunteers. *Drug Metab Dispos.* 2000;28:308–314.

OPEN ACCESS Freely available online

PLOS | ONE

Reduction of [^{11}C](+)3-MPB Binding in Brain of Chronic Fatigue Syndrome with Serum Autoantibody against Muscarinic Cholinergic Receptor

Shigeyuki Yamamoto[1,2], Yasuomi Ouchi[3], Daisaku Nakatsuka[1], Tsuyoshi Tahara[4], Kei Mizuno[4], Seiki Tajima[1], Hirotaka Onoe[4], Etsuji Yoshikawa[2], Hideo Tsukada[2], Masao Iwase[5], Kouzi Yamaguti[1], Hirohiko Kuratsune[6], Yasuyoshi Watanabe[1,4]*

1 Department of Physiology, Osaka City University Graduate School of Medicine, Abeno-ku, Osaka, Japan, **2** Central Research Laboratory, Hamamatsu Photonics KK, Hamakita, Shizuoka, Japan, **3** Molecular Imaging Frontier Research Center, Hamamatsu University School of Medicine, Hamamatsu, Japan, **4** RIKEN Center for Molecular Imaging Science (CMIS), Kobe, Hyogo, Japan, **5** Psychiatry, Department of Clinical Neuroscience, Osaka University Graduate School of Medicine, Suita, Japan, **6** Department of Health Sciences, Faculty of Health Sciences for Welfare, Kansai University of Welfare Sciences, Kashiwara, Japan

Abstract

Background: Numerous associations between brain-reactive antibodies and neurological or psychiatric symptoms have been proposed. Serum autoantibody against the muscarinic cholinergic receptor (mAChR) was increased in some patients with chronic fatigue syndrome (CFS) or psychiatric disease. We examined whether serum autoantibody against mAChR affected the central cholinergic system by measuring brain mAChR binding and acetylcholinesterase activity using positron emission tomography (PET) in CFS patients with positive [CFS(+)] and negative [CFS(−)] autoantibodies.

Methodology: Five CFS(+) and six CFS(−) patients, as well as 11 normal control subjects underwent a series of PET measurements with *N*-[^{11}C]methyl-3-piperidyl benzilate [^{11}C](+)3-MPB for the mAChR binding and *N*-[^{11}C]methyl-4-piperidyl acetate [^{11}C]MP4A for acetylcholinesterase activity. Cognitive function of all subjects was assessed by neuropsychological tests. Although the brain [^{11}C](+)3-MPB binding in CFS(−) patients did not differ from normal controls, CFS(+) patients showed significantly lower [^{11}C](+)3-MPB binding than CFS(−) patients and normal controls. In contrast, the [^{11}C]MP4A index showed no significant differences among these three groups. Neuropsychological measures were similar among groups.

Conclusion: The present results demonstrate that serum autoantibody against the mAChR can affect the brain mAChR without altering acetylcholinesterase activity and cognitive functions in CFS patients.

Citation: Yamamoto S, Ouchi Y, Nakatsuka D, Tahara T, Mizuno K, et al. (2012) Reduction of [^{11}C](+)3-MPB Binding in Brain of Chronic Fatigue Syndrome with Serum Autoantibody against Muscarinic Cholinergic Receptor. PLoS ONE 7(12): e51515. doi:10.1371/journal.pone.0051515

Editor: Francisco José Esteban, University of Jaén, Spain

Received December 29, 2011; **Accepted** September 3, 2012; **Published** December 11, 2012

Funding: This work was supported in part by Special Coordination Funds for Promoting Science and Technology, the 21st Century COE Program "Base to Overcome Fatigue" from the Japanese Ministry of Education, Culture, Sports, Science, and Technology, and grants from Japanese Ministry of Health, Labor, and Welfare. The funders had no role in study design, data collection and analysis, decision to publish, or preparation of the manuscript. No additional external funding received for this study.

Competing Interests: The authors have read the journal's policy and have the following conflicts: SY, EY and HT are employees of Hamamatsu Photonics KK. This does not alter the authors' adherence to all the PLOS ONE policies on sharing data and materials.

* E-mail: yywata@riken.jp

Introduction

Neurotransmission at the muscarinic cholinergic receptor (mAChR) in the central nervous system is involved in cognitive function [1–3], motor control [4,5], and rapid eye movement sleep [6]. Abnormalities of the central mAChR system in Alzheimer's disease correlate well with the degree of dementia [7–9]. Postmortem studies have shown that reductions in central mAChR systems were present not only in Alzheimer's-type dementia [10,11] but also in Huntington's disease [12–14], Parkinson's disease [15], and schizophrenia [16–18]. Five subtypes of mAChR, M_{1-5}, have been identified by molecular cloning [19], and the M_1 receptor has a significant role in cognitive function [3,20]. These results suggest that the activity of the mAChR M_1 plays a role in maintenance of cognitive function in neuropsychiatric diseases.

In recent years, numerous brain-reactive antibodies have been identified in human sera and have been proposed to relate to neurological or neuropsychiatric symptoms [21–23]. Even when antibodies are present in serum, the blood-brain barrier (BBB) prevents an influx of antibodies into the brain tissues in the healthy condition. In contrast, BBB compromise permits the influx of antibodies into the brain and induces neuropsychiatric symptoms in experimental animals [24].

Chronic fatigue syndrome (CFS) is a heterogeneous disorder characterized by persistent fatigue accompanied by rheumatologic, cognitive, and infectious-appearing symptoms [25,26]. CFS research showed abnormal cytokine levels including tumour

necrosis factor, interleukin-1, interleukin-6 [27], increased markers of inflammation [28] and stressful life events prior to CFS onset [29,30]. It has been established through *in vitro* and *in vivo* studies that BBB function was disrupted by tumour necrosis factor, interleukin-1 and interleukin-6 [31–34]. The BBB is also impaired by local inflammation [35] and stress [36]. Therefore, CFS patients might have some BBB impairment. Increased levels of the serum autoantibody against the mAChR M_1 have been reported in CFS patients [37].

These lines of evidence led us to investigate the effect of autoantibody against the mAChR on the muscarinic cholinergic system in the brain *in vivo*. The mAChR was evaluated using a positron emission tomography (PET) ligand *N*-[^{11}C]methyl-3-piperidyl benzilate ([^{11}C](+)3-MPB) [38], and acetylcholinesterase (AChE) activity was assessed with *N*-[^{11}C]Methyl-4-piperidyl acetate ([^{11}C]MP4A) [39–41].

Materials and Methods

Ethics

All subjects gave their written, informed consent to participate in the present study. The study was approved by the Ethics Committee of Osaka City University Graduate School of Medicine (Osaka, Japan) and Hamamatsu Medical Center (Hamamatsu, Japan).

Objective

The aim of the present study was to investigate the effect of serum autoantibody of mAChR on brain functions in CFS by comparing the central cholinergic system among CFS patients with positive (CFS(+)) and negative (CFS(−)) autoantibody against the mAChR.

Participants

The serum samples from CFS patients were assayed for the autoantibody against the mAChR. All CFS patients included in this study were diagnosed according to the clinical diagnostic criteria [26] at Osaka City University Hospital (Osaka, Japan). Patients were divided into CFS(+) and CFS(−) groups according to the assay for the autoantibody against the mAChR (described below). Five CFS(+) patients (3 female and 2 male, 39.2±7.0 years old), 6 CFS(−) patients (3 female and 3 male, 32.0±2.5 years old), and 11 healthy controls (5 female and 6 male, 32.9±6.5 years old) took part in the PET study (Table 1). All study participants were Asian. All the patients were medicated with vitamin C and the Chinese herbal medicine hochuekkito. There is no evidence that vitamin C and hochuekkito affect mAChR in the brain. The exclusion criteria for study participation were smoking, drinking alcohol regularly and taking medications known to affect the central cholinergic system including AChE inhibitors. Control subjects were neurologically and psychiatrically normal and had no history of medication or drug or alcohol dependence.

Description of Procedures

Serum samples were collected on the PET experimental day, and assayed for the autoantibody against the mAChR again to confirm the reliability of the immunoassay. After the acquisition of magnetic resonance images (MRI), PET experiments were performed. On the same day, patients filled out a questionnaire about the extent of fatigue [using a by the visual analogue scale] [42]. All participants underwent comprehensive neuropsychological tests. Predictive IQ was assessed by the Japanese version of the National Adult Reading Test [43]. Measurements of executive functions were obtained with the Wisconsin Card Sorting Test [44] and Advanced Trail-Making Tests, which was a touch panel version of the original trail-making test [45]. The Advanced Trail-Making Tests have been used as a task to measure mental fatigue [46,47]. Non-verbal long term memory was assessed by the Rey Complex Figure test [48]. Finally, memory function was assessed comprehensively by the full version of the Japanese Wechsler Memory Scale-Revised [49].

Detection of Autoantibody to mAChR by Radioligand Assay

The radioligand assay was conducted according to methods described in our previously published study [37]. The open reading frame of mAChR was obtained by reverse transcript polymerase chain reaction (PCR) amplification using poly-A RNA from the human hippocampus (CLONTECH Laboratories, Palo Alto, CA) as a template. The first strand cDNA was synthesized using ReverTraAce (TOYOBO, Tokyo, Japan) with random hexamers according to the manufacturer's instructions. PCR using the following primer pairs containing either an EcoRI or an XhoI site. 5′-GGAATTCATGAACACTTCAGCCCCACCTGC-3′ and 5′-CCGCTCGAGTCAGCATTGGCGGGAGGGAGT-3′ (the EcoRI and XhoI sites have been underlined) was used. PCR was carried out using KOD-plus (TOYOBO) as a DNA polymerase. Each cDNA was digested with an EcoRI and an XhoI and ligated into the pET28a(+) expression vector (Novagen, Madison, WI). The [^{35}S]-methionine-labeled protein was produced using cDNA, TNT Quick coupled Transcription/Translation System (Promega, Madison, WI), and [^{35}S]-methionine (Amersham Biotech, Arlington Heights, IL) according to the manufacturer's instructions. The [^{35}S]-methionine-labeled protein was then applied to a Nick column (Amersham Biotech) to remove free [^{35}S]-methionine, electrophoresed to SDS-PAGE (15%

Table 1. Demographic overview of control and CFS patients.

Variable	Control	CFS(−)	CFS(+)
N	11	6	5
Sex (female/male)	5/6	3/3	3/2
Age (years)	32.9±6.5	32.0±2.5	39.2±7.0
Extent of fatigue expressed by visual analogue scale, mean ± SD	1.1±0.7	6.7±1.4***	5.9±1.2***

Data are expressed as mean ± SD.
***p<0.001, significantly different from the corresponding values for the control (one way ANOVA using a post hoc Student-Newman-Keuls test).
doi:10.1371/journal.pone.0051515.t001

polyacrylamide gel), and autoradiography demonstrated the presence of a band component for the mAChR.

The [^{35}S]-labeled human mAChR protein was diluted to 1000 counts per minute (cpm) per microliter by reaction buffer (50 mmol/l Tris-HCl, 150 mmol/l NaCl, 0.1% BSA, 0.1% Tween-20, and 0.1% NaN_3, pH 7.4) and stored at −80 C until use. Ten microliters of a patient's sera were diluted with 490 µl of reaction buffer. Thirty microliters of diluted patient sera and 20 µl of reaction buffer containing 20,000 cpm of [^{35}S]-labeled human mAChR protein were incubated overnight at 4°C. The final dilution of each serum sample was 1:50. The reaction mixtures were transferred to each well in a 96-well filtration plate (Millipore, Benford, MA), which had been pretreated with blocking buffer (50 mmol/l Tris-HCl, 150 mmol/l NaCl, 3% BSA, and 0.1% NaN_3, ph 7.4) at 4°C overnight. Ten microliters of 50% protein G Sepharose 4FF (Amersham Bioscience) was added to each well to isolate the immune complex and then incubated for 45 min at room temperature. The plate was washed 10 times with 200 µl washing buffer (50 mmol/l Tris-HCl, 150 mmol/l NaCl, and 1% Tween-20, pH 7.4) using a vacuum manifold (Millipore). The filter was dried and OptiPhase SuperMix (Perkin-Elmer Life Science, Boston, MA) was added to each well before the quantity of precipitated labeled protein was counted in a 1450 MicroBeta TriLux apparatus (Perkin-Elmer Life Science). All samples were measured in duplicate. The inter-assay coefficient of variation varied from 6.3% to 9.6%.

The results were expressed as an antibody index and were calculated as follows:

$$\text{AntibodyIndex} = \frac{[\text{cpm of the sample serum}] - [\text{cpm of the normal serum}]}{[\text{cpm of the positive standard serum}] - [\text{cpm of the normal pooled serum}]} \times 100$$

Commericial antibodies to human mAChR M_1 (C-20) (Santa Cruz Biotechnology, Santa Cruz, CA) was used as the positive standard for anti-mAChR antibody. The cut-off value was calculated as the mean±2 S.D. in healthy controls.

MRI and PET Experiments

MRI with 3D mode data acquisition was performed on a 3.0-T scanner (MRP7000AD, Hitachi, Tokyo, Japan) to determine the brain areas for setting the regions of interests (ROIs). MRIs from each subject revealed no apparent morphological abnormalities.

We used [^{11}C](+)3-MPB to evaluate the activity of brain mAChR in the present PET study. In 1998, a human PET study with [^{11}C](+)3-MPB had already been carried out under the approval of the local committee of the prefectural Research Institute for Brain and Blood Vessels in Akita [50]. In 2004, the Ethics Committee of Hamamatsu Medical Center approved our PET study with [^{11}C](+)3-MPB, based on the approval of the human study performed by Takahashi and colleagues in a public facility. After the approval, we performed the current human PET study from 2004 to 2010, during which we tried hard to seek for patients with our criteria. In 2011, we planned another PET study with [^{11}C](+)3-MPB in collaboration with other groups, and the collaborators requested us to re-examine the safety of (+)3-MPB because they wondered if the first precursor of [^{11}C](+)3-MPB we had used in the human study was good enough to be used in their study. So, we asked Nard Institute Ltd to do the safety test (study number CG11117), and confirmed the safetiness.

PET was performed as described previously [42] on a brain SHR12000 tomograph (Hamamatsu Photonics KK, Hamamatsu, Japan) having an intrinsic resolution of 2.9×2.9×3.4 scanner in full width at half maximum, 47 slices, and a 163-mm axial field of view. Two PET measurements using [^{11}C](+)3-MPB and [^{11}C]MP4A were performed sequentially at 3-hour intervals on the same day. The order of [^{11}C](+)3-MPB and [^{11}C]MP4A PET measurements were counterbalanced across subjects. The specific radioactivities of these ligands were found to be more than 50 GBq/µmol after synthesis of [^{11}C](+)3-MPB and [^{11}C]MP4A, respectively.

After head fixation using a thermoplastic face mask, a 10-min transmission scan for attenuation correction was obtained. After a bolus injection of [^{11}C](+)3-MPB (348.9±57.2 MBq), serial PET scans were performed with a total duration of 92 min (4×30 sec, 20×1 min, and 14×5 min). After a bolus injection of [^{11}C]MP4A (297.6±53.8 MBq), serial PET scans were performed for a total of 62 min (4×30 sec, 20×1 min, and 8×5 min).

PET Data Analysis

The brain MRI was first co-registered to the PET image by pixel-wise kinetic modeling software (Pixel-Wise Kinetic Modeling Group, Zurich, Switzerland). The following ROIs were drawn bilaterally on the registered MR images; dorsolateral prefrontal cortex, anterior cingulate cortex, amygdala, occipital cortex, parietal cortex, temporal cortex, orbitofrontal cortex, thalamus and cerebellum. These ROIs were then transferred onto the corresponding dynamic [^{11}C](+)3-MPB images and static [^{11}C]MP4A image.

For [^{11}C](+)3-MPB analysis, the Logan reference tissue method was used in pixel-wise kinetic modeling software. In this study, the cerebellum was used as the reference region [51]. The Logan reference tissue method allows the estimation of the distribution volume ratio (DVR), which can be expressed as follows [52]:

$$\int_0^T ROI_{tar}(t)dt / ROI_{tar}(T) = DVR[\{\int_0^T ROI_{ref}(t)dt / ROI_{ref}(T)/k_2\} ROI_{tar}(T)] + C$$

where ROI_{tar} and ROI_{ref} are the radioactivity concentrations of the target and reference region, respectively, at time-T. The DVR is the slope and k_2 is the clearance rate from the reference region. A k_2 value of 0.31 was used, according to a previous study [51]. C is the intercept of the Y-axis. The DVR is the ratio of the distribution volume in the target to the reference region. DVR minus one was calculated as BP_{ND}, which is the ratio at equilibrium of specifically bound radioligand to that of non-displaceble radioligand (ND) in tissue [53]. Data recorded during the first 15 min were excluded based upon our previous PET study [38]. We also generated parametric images of the binding potential (BP_{ND}) by the Logan reference tissue method based on pixel-wise kinetic modelling [54].

For [^{11}C]MP4A analysis, the summation image from 32–62 min postinjection was obtained, and the uptake values in target ROIs divided by the uptake of the cerebellar hemisphere was used for the AChE activity ([^{11}C]MP4A index) [55,56].

Statistics

The age, extent of fatigue, results of neuropsychological tests, and regional BP_{ND} values or uptake were compared among 3 groups with one way ANOVA using a post hoc Student-Newman-Keuls test. Statistical significance was set at $P<0.05$.

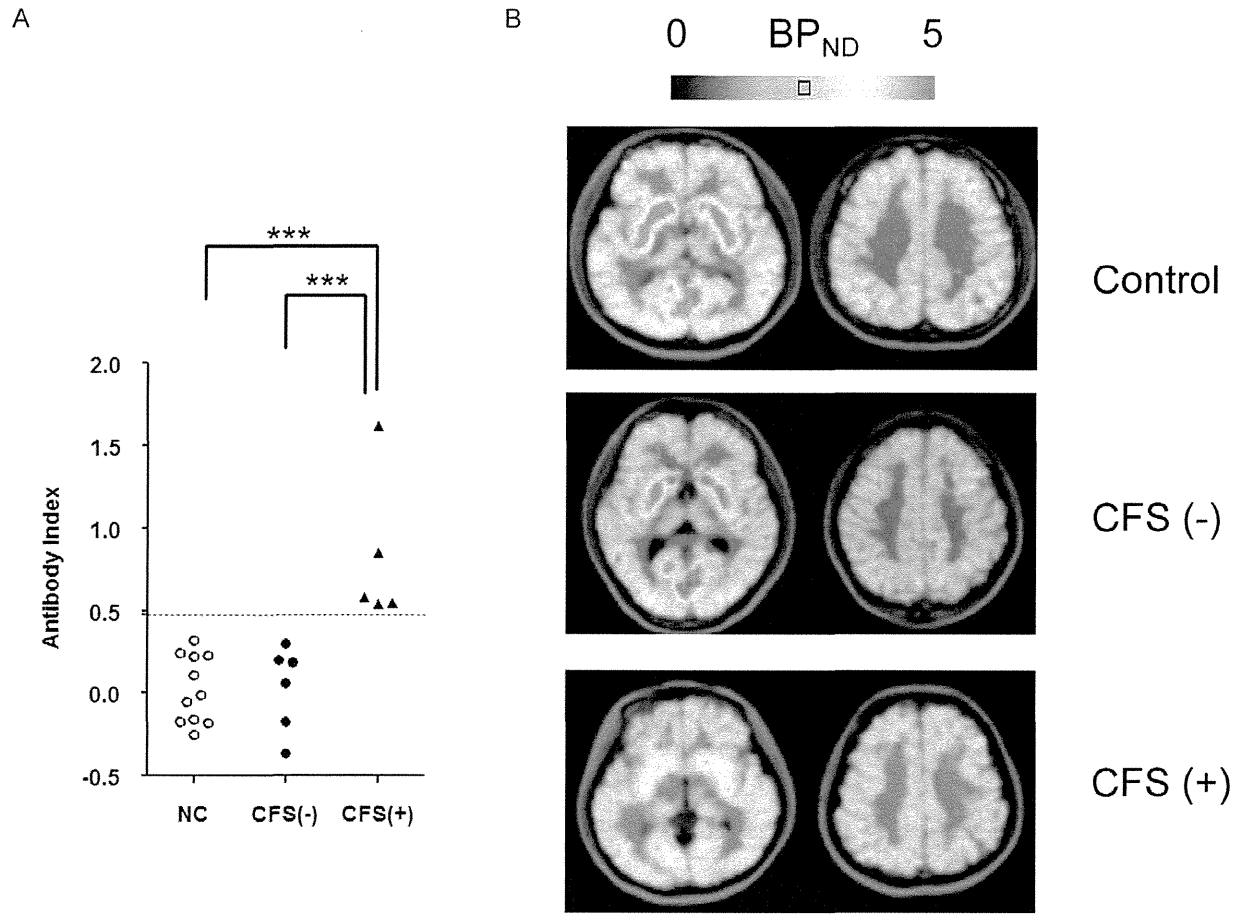

Figure 1. Serum autoantibody and PET images with [^{11}C](+)3-MPB among normal control (NC) and CFS(−) and CFS(+) patients. (A) Antibody index against the muscarinic cholinergic receptor (mAChR) in serum from NC, CFS(−) and CFS(+) groups. ***p<0.001, significantly different from the corresponding value for the CFS(+) patients (one way ANOVA using a post hoc Student-Newman-Keuls test). (B) Representative parametric PET images of [^{11}C](+)3-MPB binding in NC, CFS(−) and CFS(+) groups.
doi:10.1371/journal.pone.0051515.g001

Table 2. Results of neuropsychological tests.

Test	Control	CFS(−)	CFS(+)
Japanese version of the National Adult Reading Test	72.0±11.1	79.3±13.7	75.4±9.3
Advanced Trail-Making Test A	124.3±28.7	125.1±19.2	125.5±30.7
Advanced Trail-Making Test B	163.2±34.6	161.5±31.2	187.4±70.1
Advanced Trail-Making Test C	263.9±45.0	260.8±45.8	275.7±27.0
Rey Complex Figure: immediate recall	28.7±2.5	29.8±2.7	28.7±3.3
Rey Complex Figure: delayed recall	28.0±3.3	28.7±3.1	27.8±2.7
Wisconsin Card Sorting Test	327.5±108.1	314.7±41.7	338.2±106.8
Wechsler Memory Scale-Revised			
General memory	112.1±8.0	114.5±9.4	109.2±5.3
Delayed memory	113.8±9.0	115.0±11.2	112.4±6.5
Verbal memory	109.7±9.1	112.0±10.6	107.0±7.0
Visual memory	114.0±5.5	114.7±5.2	113.2±6.3
Attention	102.0±14.6	100.5±16.6	103.8±13.5

Data are expressed as mean ± SD.
No significant differences were observed among control, CFS(−), and CFS(+) patients.
doi:10.1371/journal.pone.0051515.t002

Results

Figure 1A shows the radioligand assay in serum samples collected on the PET experiment day. There were 5 positive patients (CFS(+)) whose serum autoantibody was higher than the cut-off value shown as a dashed line. In normal controls, there were no subjects with positive autoantibody against the mAChR. As shown in Table 1, fatigue scores, expressed by visual analogue scale, were similar between CFS(+) and CFS(−) patients (5.9±1.2 vs. 6.7±1.4, respectively). In all the neuropsychological assessments, there were no significant differences among the 3 groups (Table 2).

Representative maps of the BP_{ND} of [^{11}C](+)3-MPB using the Logan plot with reference regions are presented in Figure 1B. The BP_{ND} of [^{11}C](+)3-MPB in each brain of CFS(+) patients were significantly lower than those in CFS(−) patients and control subjects (Fig. 1B, Table 3). Compared with controls, a 10–25% reduction of BP_{ND} was observed in CFS(+) patients (Table 3). AChE activity did not differ among the 3 groups (Table 3). There were no significant differences in BP_{ND} between CFS(−) patients and control subjects. There were no regions in which the BP_{ND} of [^{11}C](+)3-MPB significantly correlated with any neuropsychological indices.

Discussion

Reduction of [^{11}C](+)3-MPB binding was observed in CFS(+) patients who showed a higher level of serum autoantibody against the mAChR, compared with CFS(−) patients and normal controls. In contrast, the AChE activity was similar in subjects from the 3 groups. The indices of intelligence and cognitive function did not differ among the 3 groups, and these indices did not relate to [^{11}C](+)3-MPB binding in this study. To our knowledge, this is the first PET study to demonstrate a reduction of neurotransmitter receptor binding in brains of CFS patients with high levels of serum autoantibody. The present results suggest the possibility of the autoantibody interacting directly with the mAChR in the brain, although the autoantibody at this level did not affect cognitive function in CFS patients. The present finding supports the idea that penetration of the antibody into the brain resulted in impaired BBB function. This may be one possible mechanism by which the serum autoantibody could affect central mAChR function [57].

Although the precise mechanism of the production of the autoantibodies against the mAChR in the CFS brain is unclear, there are the following mechanisms based on an autoimmune reaction theory: 1) a viral infection of the brain tissue exposes the brain to self-antigen; and 2) an infection (not necessarily in the brain tissue) causes production of antibodies which, as a result of molecular mimicry, identify brain antigens as non-self and cause

Table 3. Comparisons of [^{11}C](+)3-MPB BP_{ND} and [^{11}C]MP4A index among control, CFS(−) and CFS(+) groups.

	[^{11}C](+)3-MPB BP_{ND}			
ROI	**Control**	**CFS(−)**	**CFS(+)**	**Reduction (%)**
Dorsolateral Prefrontal Cortex	2.74±0.40	2.65±0.20	2.19±0.29* #	20
Anterior Cingulate Cortex	2.87±0.39	2.93±0.37	2.26±0.50* #	21
Orbitofrontal Cortex	2.71±0.30	2.79±0.21	2.14±0.35** ##	21
Temporal Cortex	2.57±0.24	2.61±0.22	2.24±0.28* #	13
Parietal Cortex	2.47±0.33	2.66±0.19	2.12±0.29* #	14
Occipital Cortex	2.60±0.28	2.69±0.27	2.25±0.24* #	14
Striatum	4.73±0.60	4.70±0.50	3.69±0.75* #	22
Thalamus	1.73±0.18	1.82±0.10	1.51±0.22* #	13
Amygdala	2.20±0.36	2.32±0.22	1.66±0.19** ##	25
Brainstem	0.95±0.15	0.92±0.16	0.86±0.15* #	10
	[^{11}C]MP4A index			
Dorsolateral Prefrontal Cortex	0.43±0.04	0.43±0.03	0.44±0.02	−4
Anterior Cingulate Cortex	0.50±0.05	0.51±0.05	0.49±0.02	1
Orbitofrontal Cortex	0.49±0.05	0.47±0.04	0.47±0.03	3
Temporal Cortex	0.42±0.03	0.43±0.03	0.43±0.02	−2
Parietal Cortex	0.38±0.03	0.39±0.03	0.40±0.01	−6
Occipital Cortex	0.37±0.03	0.38±0.03	0.38±0.02	−4
Striatum	–	–	–	–
Thalamus	0.82±0.07	0.77±0.07	0.85±0.04	−4
Amygdala	0.64±0.05	0.61±0.07	0.64±0.04	1
Brainstem	0.84±0.06	0.87±0.07	0.82±0.05	2

Data are expressed as mean ± SD.
*p<0.05,
**p<0.01, significantly different from the corresponding values for the control.
#p<0.05,
##p<0.01, significantly different from the corresponding values for the CFS(−).
Reduction (%) reflects the extent of decreased in the rates of [^{11}C](+)3-MPB BP_{ND} or [^{11}C]MP4A index from control to CFS(+).
doi:10.1371/journal.pone.0051515.t003

autoimmune reactions [58]. These mechanisms are plausible because a series of viruses such as the Epstein-Barr virus, human herpes virus 6, group B coxsackie virus, human T-cell lymphotrophic virus II, hepatitis C, enteroviruses and retroviruses were found to act as etiological agents for CFS [59]. Therefore, it is very likely that autoantibodies develop in some populations of CFS patients.

There are some possible reasons for the reduction of [^{11}C](+)3-MPB binding in CFS(+) patients. First, the autoantibody may have penetrated through the impaired BBB directly destroying the mAChR in the brain. A second possibility is that increased endogenous acetylcholine (e.g. resulting from inhibition of AChE activity) competes with [^{11}C](+)3-MPB at the mAChR. However, the latter seems unlikely. Our previous PET study showed that [^{11}C](+)3-MPB did not compete with endogenous acetylcholine because of its high affinity for the receptors [60]. In addition, the present results indicate no significant changes in AChE activity assessed with [^{11}C]MP4A, even in CFS(+) patients. A third possible mechanism underlying reduced [^{11}C](+)3-MPB binding is that antibodies may act as receptor agonists or antagonists [21]. It was reported that serum autoantibodies against the mAChR displayed agonist-like activity, such as increased cGMP production, activated phosphoinositide turnover, and translocated protein kinase C [61]. All of these biological effects resemble the effects of the mAChR agonists like pilocarpine, and were minimized by the mAChR antagonist pirenzepine. In addition, the agonistic activity by these autoantibodies might induce desensitization, internalization and/or intracellular degradation of the mAChR, resulting in a progressive decrease of the mAChR expression in the brain [62]. Taken together, the present results suggest that autoantibodies penetrating the BBB from the serum to the brain may act on the mAChR directly and specifically in the CFS brain without altering AChE activity.

Five subtypes of mAChR, M_{1-5}, have been identified by molecular cloning [19]. M_1, M_2 and M_4 receptors are predominant subtypes expressed in different percentages among brain regions. Quantitative immunoprecipitation study indicates that the distribution percentages of M_1, M_2 and M_4 receptors are 60%, 20% and 20% in the cortex, respectively. In the striatum, their distribution percentages are 30%, 20% and 50%, respectively [63]. We had expected a greater reduction of [^{11}C](+)3-MPB BP_{ND} in the cortex than in the striatum because serum autoantibody detected in the present study was specific for the M_1 receptor. However, similar reductions in the rate of [^{11}C](+)3-MPB BP_{ND} were observed between the cortex and striatum (Table 3). One possible explanation for this is the low selectivity of [^{11}C](+)3-MPB to the subtype of mAChR. The Ki values of (+)3-MPB for the human receptors from M_1 to M_5 were 1.34, 1.17, 2.82, 1.76, and 5.91 nM, respectively, as assessed with five cloned human mAChR subtypes expressed in CHO-K1 cells (unpublished data). These data indicate that the M_1 receptor and the other subtype of mAChR contribute to the reduction in the rate of [^{11}C](+)3-MPB BP_{ND} in CFS(+) patients.

Because the M_1 receptor has a significant role in cognitive function [3,20], we predicted cognitive impairment in CFS(+) patients. However, cognitive function in CFS patients was not associated with changes in [^{11}C](+)3-MPB BP_{ND}. One plausible explanation is that reduction in the level of [^{11}C](+)3-MPB BP_{ND} occurs within a range of preserved cognitive function. Indeed, we recently reported the relationship between [^{11}C](+)3-MPB BP_{ND} and cognitive function in conscious monkeys, showing that there were thresholds (ca. 30–40% in cortex and ca. 20–30% in brainstem) of activity of the brain mAChR to induce cognitive impairment [64,65].

Limitations

We cannot exclude the possibility that the autoimmune reaction occurred as a secondary process to the reduction of the mAChR. In addition, our findings relate to a small subset of CFS patients. This was chiefly due to the difficulty in obtaining CFS patients' consent to participate in the present study because it entailed a series of PET and MRI measurements, requiring a significant commitment of time from each subject. Additional experiments will be necessary to fully validate the present findings. Increases in the serum autoantibody against the mAChR have also been reported in Sjögren syndrome [66] and other psychiatric disorders including schizophrenia [61,62,67]. Therefore, our results cannot be generalized to the entire CFS population.

Summary

Our results demonstrate the usefulness of PET as a tool for detecting a reduction of neurotransmitter receptor binding in the brains of patients with high levels of serum autoantibody. Further follow up studies on a number of CFS patients are required in order to more thoroughly investigate alterations in cholinergic and neuronal functions with regard to levels of mAChR autoantibody and clinical symptoms.

Acknowledgments

The authors thank the participants and the technical support team in charge of blood sampling.

Author Contributions

Conceived and designed the experiments: YW. Performed the experiments: SY YO DN TT ST EY HT MI KY HK. Analyzed the data: SY TT KM ST EY. Wrote the paper: SY YO KM HO YW.

References

1. Collerton D (1986) Cholinergic function and intellectual decline in Alzheimer's disease. Neuroscience 19: 1–28.
2. Hasselmo ME (2006) The role of acetylcholine in learning and memory. Curr Opin Neurobiol 16: 710–715.
3. Sellin AK, Shad M, Tamminga C (2008) Muscarinic agonists for the treatment of cognition in schizophrenia. CNS Spectr 13: 985–996.
4. Kobayashi Y, Inoue Y, Yamamoto M, Isa T, Aizawa H (2002) Contribution of pedunculopontine tegmental nucleus neurons to performance of visually guided saccade tasks in monkeys. J Neurophysiol 88: 715–731.
5. Matsumura M, Watanabe K, Ohye C (1997) Single-unit activity in the primate nucleus tegmenti pedunculopontinus related to voluntary arm movement. Neurosci Res 28: 155–165.
6. Steriade M (1992) Basic mechanisms of sleep generation. Neurology 42: 9–17.
7. Höhmann C, Antuono P, Coyle JT (1998) Basal forebrain cholinergic neurons and Alzheimer's disease. In: Iversen LL, Iversen SD, Snyder SD, editors. Psychopharmacology of the aging nervous system. New York: Plenum. 69–106.
8. Perry EK (1986) The cholinergic hypothesis–ten years on. Br Med Bull 42: 63–69.
9. Terry AV Jr, Buccafusco JJ (2003) The cholinergic hypothesis of age and Alzheimer's disease-related cognitive deficits: recent challenges and their implications for novel drug development. J Pharmacol Exp Ther 306: 821–827.
10. Reinikainen KJ, Riekkinen PJ, Halonen T, Laakso M (1987) Decreased muscarinic receptor binding in cerebral cortex and hippocampus in Alzheimer's disease. Life Sci 41: 453–461.
11. Rinne JO, Laakso K, Lönnberg P, Mölsä P, Paljärvi L, et al. (1985) Brain muscarinic receptors in senile dementia. Brain Res 336: 19–25.
12. Enna SJ, Bird ED, Bennett JP Jr, Bylund DB, Yamamura HI, et al. (1976) Huntington's chorea. Changes in neurotransmitter receptors in the brain. N Engl J Med 294: 1305–1309.
13. Lange KW, Javoy-Agid F, Agid Y, Jenner P, Marsden CD (1992) Brain muscarinic cholinergic receptors in Huntington's disease. J Neurol 239: 103–104.

14. Wastek GJ, Yamamura HI (1978) Biochemical characterization of the muscarinic cholinergic receptor in human brain: alterations in Huntington's disease. Mol Pharmacol 14: 768–780.
15. Ahlskog JE, Richelson E, Nelson A, Kelly PJ, Okazaki H, et al. (1991) Reduced D2 dopamine and muscarinic cholinergic receptor densities in caudate specimens from fluctuating parkinsonian patients. Ann Neurol 30: 185–191.
16. Crook JM, Tomaskovic-Crook E, Copolov DL, Dean B (2000) Decreased muscarinic receptor binding in subjects with schizophrenia: a study of the human hippocampal formation. Biol Psychiatry 48: 381–388.
17. Dean B, McLeod M, Keriakous D, McKenzie J, Scarr E (2002) Decreased muscarinic1 receptors in the dorsolateral prefrontal cortex of subjects with schizophrenia. Mol Psychiatry 7: 1083–1091.
18. Zavitsanou K, Katsifis A, Mattner F, Huang XF (2004) Investigation of m1/m4 muscarinic receptors in the anterior cingulate cortex in schizophrenia, bipolar disorder, and major depression disorder. Neuropsychopharmacology 29: 619–625.
19. Kubo T, Fukuda K, Mikami A, Maeda A, Takahashi H, et al. (1986) Cloning, sequencing and expression of complementary DNA encoding the muscarinic acetylcholine receptor. Nature 323: 411–416.
20. Bymaster FP, Felder C, Ahmed S, McKinzie D (2002) Muscarinic receptors as a target for drugs treating schizophrenia. Curr Drug Targets CNS Neurol Disord 1: 163–181.
21. Diamond B, Huerta PT, Mina-Osorio P, Kowal C, Volpe BT (2009) Losing your nerves? Maybe it's the antibodies. Nat Rev Immunol 9: 449–456.
22. Morshed SA, Parveen S, Leckman JF, Mercadante MT, Bittencourt Kiss MH, et al. (2001) Antibodies against neural, nuclear, cytoskeletal, and streptococcal epitopes in children and adults with Tourette's syndrome, Sydenham's chorea, and autoimmune disorders. Biol Psychiatry 50: 566–577.
23. Perlmutter SJ, Leitman SF, Garvey MA, Hamburger S, Feldman E, et al. (1999) Therapeutic plasma exchange and intravenous immunoglobulin for obsessive-compulsive disorder and tic disorders in childhood. Lancet 354: 1153–1158.
24. Diamond B, Kowal C, Huerta PT, Aranow C, Mackay M, et al. (2006) Immunity and acquired alterations in cognition and emotion: lessons from SLE. Adv Immunol 89: 289–320.
25. Afari N, Buchwald D (2003) Chronic fatigue syndrome: a review. Am J Psychiatry 160: 221–236.
26. Fukuda K, Straus SE, Hickie I, Sharpe MC, Dobbins JG, et al. (1994) The chronic fatigue syndrome: a comprehensive approach to its definition and study. International Chronic Fatigue Syndrome Study Group. Ann Intern Med 121: 953–959.
27. Lyall M, Peakman M, Wessely S (2003) A systematic review and critical evaluation of the immunology of chronic fatigue syndrome. J Psychosom Res 55: 79–90.
28. Raison CL, Lin JM, Reeves WC (2009) Association of peripheral inflammatory markers with chronic fatigue in a population-based sample. Brain Behav Immun 23: 327–337.
29. Hatcher S, House A (2003) Life events, difficulties and dilemmas in the onset of chronic fatigue syndrome: a case-control study. Psychol Med 33: 1185–1192.
30. Tanaka M, Watanabe Y (2010) A new hypothesis of chronic fatigue syndrome: co-conditioning theory. Med Hypotheses 75: 244–249.
31. Argaw AT, Zhang Y, Snyder BJ, Zhao ML, Kopp N, et al. (2006) IL-1beta regulates blood-brain barrier permeability via reactivation of the hypoxia-angiogenesis program. J Immunol 177: 5574–5584.
32. Banks WA (2005) Blood-brain barrier transport of cytokines: a mechanism for neuropathology. Curr Pharm Des 11: 973–984.
33. Bauer B, Hartz AM, Miller DS (2007) Tumor necrosis factor alpha and endothelin-1 increase P glycoprotein expression and transport activity at the blood-brain barrier. Mol Pharmacol 71: 667–675.
34. Paul R, Koedel U, Winkler F, Kieseier BC, Fontana A, et al. (2003) Lack of IL-6 augments inflammatory response but decreases vascular permeability in bacterial meningitis. Brain 126: 1873–1882.
35. Schwarz MJ, Ackenheil M, Riedel M, Müller N (1998) Blood-cerebrospinal fluid barrier impairment as indicator for an immune process in schizophrenia. Neurosci Lett 253: 201–203.
36. Kuang F, Wang BR, Zhang P, Fei LL, Jia Y, et al. (2004) Extravasation of blood-borne immunoglobulin G through blood-brain barrier during adrenaline-induced transient hypertension in the rat. Int J Neurosci 114: 575–791.
37. Tanaka S, Kuratsune H, Hidaka Y, Hakariya Y, Tatsumi KI, et al. (2003) Autoantibodies against muscarinic cholinergic receptor in chronic fatigue syndrome. Int J Mol Med 12: 225–230.
38. Tsukada H, Takahashi K, Miura S, Nishiyama S, Kakiuchi T, et al. (2001) Evaluation of novel PET ligands (+)*N*-[^{11}C]methyl-3-piperidyl benzilate ([^{11}C](+)3-MPB) and its stereoisomer [^{11}C](-)3-MPB for muscarinic cholinergic receptors in the conscious monkey brain: a PET study in comparison with [^{11}C]4-MPB. Synapse 39: 182–192.
39. Irie T, Fukushi K, Namba H, Iyo M, Tamagami H, et al. (1996) Brain acetylcholinesterase activity: validation of a PET tracer in a rat model of Alzheimer's disease. J Nucl Med 37: 649–655.
40. Namba H, Iyo M, Shinotoh H, Nagatsuka S, Fukushi K, et al. (1998) Preserved acetylcholinesterase activity in aged cerebral cortex. Lancet 351: 881–882.
41. Namba H, Iyo M, Fukushi K, Shinotoh H, Nagatsuka S, et al. (1999) Human cerebral acetylcholinesterase activity measured with positron emission tomography: procedure, normal values and effect of age. Eur J Nucl Med 26: 135–143.
42. Yamamoto S, Ouchi Y, Onoe H, Yoshikawa E, Tsukada H, et al. (2004) Reduction of serotonin transporters of patients with chronic fatigue syndrome. Neuroreport 15: 2571–2574.
43. Matsuoka K, Uno M, Kasai K, Koyama K, Kim Y (2006) Estimation of premorbid IQ in individuals with Alzheimer's disease using Japanese ideographic script (Kanji) compound words: Japanese version of National Adult Reading Test. Psychiatry Clin Neurosci 60: 332–339.
44. Tsuchiya H, Yamaguchi S, Kobayashi S (2000) Impaired novelty detection and frontal lobe dysfunction in Parkinson's disease. Neuropsychologia 38: 645–654.
45. Reitan RM (1956) Trail Making Test: Manual for Administration, Scoring and Interpretation, Indianapolis.
46. Horikoshi T, Matsue K, Takahashi T, Ishii H, Yamada K, et al. (2004) Objective determination of fatigue development following sun exposure using Advanced Trail Making Test. Int J Cosmet Sci 26: 9–17.
47. Tajima S, Yamamoto S, Tanaka M, Kataoka Y, Iwase M, et al. (2010) Medial orbitofrontal cortex is associated with fatigue sensation. Neurology Research International doi: 10.1155/2010/671421.
48. Spreen O, Strauss E (1998) A compendium of neuropsychological tests – Administration, Norms and Commentary. Oxford University Press, New York.
49. Wechsler D (1987) Wechsler Memory Scale Revised. The Psychological Corporation. Harcourt Brace Jovanovich, Inc.
50. Takahashi K (1998) Development and clinical application of novel C-11-labeled ligand for imaging cholinergic muscarinic receptors in the brain with positron emission tomography. Thesis Tohoku Univ 3041: 1–54 (in Japanese).
51. Yamamoto S, Ohba H, Nishiyama S, Takahashi K, Tsukada H (2010) Validation of reference tissue model of PET ligand [^{11}C](+)3-MPB for the muscarinic cholinergic receptor in the living brain of conscious monkey. Synapse 65: 548–551.
52. Logan J, Fowler JS, Volkow ND, Wang GJ, Ding YS, et al. (1996) Distribution volume ratios without blood sampling from graphical analysis of PET data. J Cereb Blood Flow Metab 16: 834–840.
53. Innis RB, Cunningham VJ, Delforge J, Fujita M, Gjedde A, et al. (2007) Consensus nomenclature for in vivo imaging of reversibly binding radioligands. J Cereb Blood Flow Metab 27: 1533–1539.
54. Buck A, Gucker PM, Schönbächler RD, Arigoni M, Kneifel S, et al. (2000) Evaluation of serotonergic transporters using PET and [^{11}C](+)McN-5652: assessment of methods. J Cereb Blood Flow Metab 20: 253–262.
55. Eggers C, Szelies B, Bauer B, Wienhard K, Schröder H, et al. (2007) Imaging of acetylcholine esterase activity in brainstem nuclei involved in regulation of sleep and wakefulness. Eur J Neurol 14: 690–693.
56. Ota T, Shinotoh H, Fukushi K, Nagatsuka S, Namba H, et al. (2004) A simple method for the detection of abnormal brain regions in Alzheimer's disease patients using [^{11}C]MP4A: comparison with [^{123}I]IMP SPECT. Ann Nucl Med 18: 187–193.
57. Axelsson R, Martensson E, Alling C (1982) Impairment of the blood-brain barrier as an aetiological factor in paranoid psychosis. Br J Psychiatry 141: 273–281.
58. Noy S, Achiron A, Laor N (1994) Schizophrenia and autoimmunity–a possible etiological mechanism? Neuropsychobiology 30: 157–159.
59. Levy JA (1994) Viral studies of chronic fatigue syndrome. Clin Infect Dis 18: S117–120.
60. Nishiyama S, Tsukada H, Sato K, Kakiuchi T, Ohba H, et al. (2001) Evaluation of PET ligands (+)*N*-[(^{11})C]ethyl-3-piperidyl benzilate and (+)*N*-[(^{11})C]propyl-3-piperidyl benzilate for muscarinic cholinergic receptors: a PET study with microdialysis in comparison with (+)*N*-[(^{11})C]methyl-3-piperidyl benzilate in the conscious monkey brain. Synapse 40: 159–169.
61. Borda T, Perez Rivera R, Joensen L, Gomez RM, Sterin-Borda L (2002) Antibodies against cerebral M1 cholinergic muscarinic receptor from schizophrenic patients: molecular interaction. J Immunol 168: 3667–3674.
62. Ganzinelli S, Borda T, Sterin-Borda L (2006) Regulation of m1 muscarinic receptors and nNOS mRNA levels by autoantibodies from schizophrenic patients. Neuropharmacology 50: 362–371.
63. Flynn DD, Ferrari-DiLeo G, Mash DC, Levey AI (1995) Differential regulation of molecular subtypes of muscarinic receptors in Alzheimer's disease. J Neurochem 64: 1888–1891.
64. Yamamoto S, Maruyama S, Ito Y, Kawamata M, Nishiyama S, et al. (2011) Effect of oxybutynin and imidafenacin on central muscarinic receptor occupancy and cognitive function: a monkey PET study with [(^{11})C](+)3-MPB. Neuroimage 58: 1–9.
65. Yamamoto S, Nishiyama S, Kawamata M, Ohba H, Wakuda T, et al. (2011) Muscarinic receptor occupancy and cognitive impairment: a PET study with [^{11}C](+)3-MPB and scopolamine in conscious monkeys. Neuropsychopharmacology 36: 1455–1465.
66. Reina S, Sterin-Borda L, Orman B, Borda E (2004) Autoantibodies against cerebral muscarinic cholinoceptors in Sjögren syndrome: functional and pathological implications. J Neuroimmunol 150: 107–115.
67. Tanaka S, Matsunaga H, Kimura M, Tatsumi K, Hidaka Y, et al. (2003) Autoantibodies against four kinds of neurotransmitter receptors in psychiatric disorders. J Neuroimmunol 141: 155–164.

—Review—

分子イメージングを活用する早期・探索的臨床研究

渡辺恭良[a,b]

Molecular Imaging-based Early-Phase and Exploratory Clinical Research

Yasuyoshi Watanabe[a,b]

[a]RIKEN Center for Molecular Imaging Science; 6-7-3 Minatojima-minamimachi, Chuo-ku, Kobe 650-0047, Japan: and [b]Department of Physiology, Osaka City University Graduate School of Medicine; 1-4-3 Asahimachi, Abeno-ku, Osaka 545-8585, Japan.

(Received August 21, 2012)

In vivo molecular imaging became a key technology for innovative drug development. Especially, positron emission tomography (PET) has been applied to patho-physiological science, pharmacodynamics/pharmacokinetics (PD/PK) studies, and drug delivery system (DDS) studies, and accelerated the paradigm shift not only from experimental animals to human subjects, but also from PK in blood circulation to PK in target tissues, even in human. Our RIKEN Centre for Molecular Imaging Science has been established to promote such innovative drug developmental studies with PET molecular imaging, as a center of excellence for development of molecular probes. The center is creating novel labeling methods on drug candidate molecules with positron-emitting radionuclides, and is providing the molecular probes suitable for targeting bio-functional molecules and cellular functions, which are useful for evaluation of drug efficacy and pharmacokinetics in human subjects. Animal PET studies with mice, rats, rabbits, marmosets, and macaque monkeys have also been promoted both under anesthetic condition and consciousness, which was a really difficult task but important for comparison with human PET studies. In this sense, mutual collaboration between the research consortia in basic PET field and in clinical PET molecular imaging such as Osaka City University Hospital would be of great value. Here, the concept, outline of our activities, and PK/PD studies with efficient application of molecular imaging is presented. In addition, the results of the first cassette-dose and micro-dose clinical trials approved by Pharmaceuticals and Medical Devices Agency (PMDA) (New Energy and Industrial Technology Development Organization (NEDO) project represented by Prof. Yuichi Sugiyama) are described.

Key words——molecular imaging; positron emission tomography (PET); pharmacokinetics; pharmacodynamics; drug delivery system; micro-dose clinical trial

1. 分子イメージング拠点構想，研究体制と活動現況

ポストゲノム時代に入り，ライフサイエンス研究の主要ターゲットは遺伝情報の解読研究から生体分子機能を探る研究に移り，分子イメージング研究はこのパラダイムシフトを担う重要な研究分野と考えられている．生きて機能している対象に対するライヴサイエンス（Live Science）が志向される．

The author declares no conflict of interest.

[a]理化学研究所分子イメージング科学研究センター（〒650-0047 神戸市中央区港島南町 6-7-3），[b]大阪市立大学大学院医学研究科システム神経科学（〒545-8585 大阪市阿倍野区旭町 1-4-3)
e-mail: yywata@riken.jp

本総説は，日本薬学会第 132 年会シンポジウム S22 で発表したものを中心に記述したものである．

われわれは，これまでに，科学技術振興機構の国際共同研究(1993-1997 年，研究代表者：渡辺恭良，http://www.jst.go.jp/icorp/jpn/past_proj/sub.html)，日本学術振興会の未来開拓学術研究事業（1998-2003 年，プロジェクトリーダー：渡辺恭良），文部科学省学術創成研究（2001-2006 年，研究リーダー：鈴木正昭岐阜大学教授，サブリーダー：渡辺恭良）のプロジェクトを中心に positron emission tomography（PET）を用いた分子イメージング研究を行い，多数の標的分子をイメージングするための分子プローブ作りを行ってきた．数々の成功例は出てきたが，ライフサイエンス研究領域や創薬研究領域で，さらに多数のバイオマーカーを追跡する需要が大きくなり，一層効率のよい分子プローブ設計・合成とそのイメージングによる評価を統合した

研究体制とそのための拠点作りが肝要になってきた．そこで，文部科学省により，平成17年（2005年）度から，分子イメージングプログラムが開始され，創薬候補物質探索拠点として理化学研究所が，PET疾患診断研究拠点として放射線医学総合研究所が選出された．平成21年度をもって5年間の第1期の成果を上げ，後継の「分子イメージング研究戦略推進プログラム（J-AMP）」が平成22年度より動き出して，両拠点の研究活動をさらに活用して，「難治がん」と「認知症」における臨床研究でのproof of concept（POC）を築くことを目標としている．

わが国が国際社会を牽引して発展すべき分子イメージング研究を阻害する一番の要因は，新しい化合物をfirst-in-human試験へ導入する際の試験体制の整備（欧州型のmicrodosing concept，あるいは，米国Food and Drug Administration（FDA）型のexploratory IND）であったが，その点も，All Japanの指針が固まり，厚生労働省のマイクロドーズ臨床試験指針作成班での討議を受け，2008年6月に厚生労働省よりマイクロドーズ臨床試験のガイダンスが公表された．ついで，2009年6月に日米欧三極の医薬品規制調和国際会議（International Conference on Harmonisation of Technical Requirements for Registration of Pharmaceuticals for Human Use; ICH）で合意されたM3(R2)文書には，「早期探索的臨床試験」の方法論が盛り込まれ，わが国では2010年2月に公示された．この早期探索的臨床試験の中に，マイクロドーズ臨床試験とともに，もう少し投与量を高く設定できる，準薬効用量と薬効用量の試験法が述べられている．この薬効用量の試験にPET分子イメージングを融合すると，疾患への有効性や安全性の見極めを臨床開発の初期段階に行うことが可能になる．

この期において，ますます効率よい標識化合物の合成法を開発し，従来の低分子化合物ばかりでなく，抗体医薬，核酸医薬，ひいては，ゲノム創薬につながるevidence-based medicine（EBM）のために，高分子物質にまで分子プローブレパートリーを広げ，ほとんどの分子を生体で追跡できるプラットフォームを構築していくことが重要である．そのような目的で，理化学研究所分子イメージング科学研究センター（http://www.cmis.riken.jp/）では，

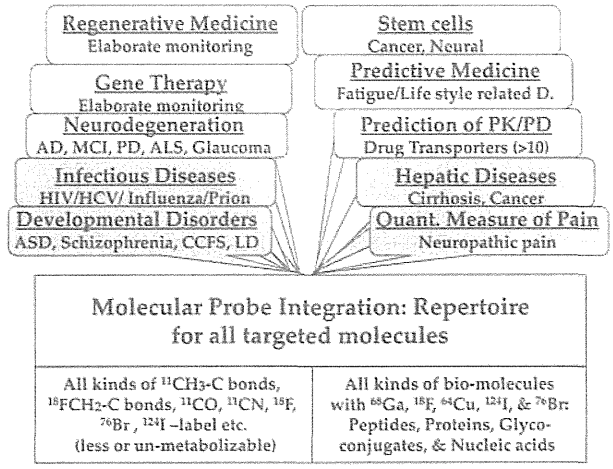

Fig. 1. Mission and Collaboration Theme/Projects of RIKEN Center for Molecular Imaging Science

Fig. 1のようなミッションと様々な共同研究先をも包含した研究テーマを持っている．化学と動物実験に秀でている研究機関であり，世界を見渡しても有数のユニークな研究センターである．本施設をセットアップし，本格的な標識化合物作りを始めてからここ5年間で，既に，140種以上の新規オリジナルPETプローブを創製し，50種を現在手がけて合成を進めており，また，既知の分子イメージングプローブ約62種を利用可能にした．現時点で，合計202種以上の分子プローブレパートリーを利用できる．今後，さらに多くのレパートリーの化合物が使える公算で，例えば，脳のほとんどすべての神経伝達系を追跡できる技術が完成すると，現在はまだアプローチできていないほとんどの神経系の相互作用や協奏作用の研究に歩を進めることができる．統合的ライフサイエンス（ライヴサイエンス）研究に欠くべからざる技術である．これらの技術や創製分子プローブを臨床の場，創薬研究の場に提供していくことが本センターの重要なミッションである．た

渡辺恭良

1976年京都大学医学部卒，1980年同博士課程修了，1981年京都大学・助手，1984年大阪医科大学・講師，1987–2001年大阪バイオサイエンス研究所・研究部長，1999年より現在まで大阪市立大学大学院医学研究科・教授，2006年から，理化学研究所分子イメージング研究プログラムディレクター，2008年から同分子イメージング科学研究センター長，日本疲労学会理事長，日本分子イメージング学会運営委員ほか．ベルツ賞，文部科学大臣表彰等受賞．